



NRL/MR/6110--10-9234

# **EMI Array for Cued UXO Discrimination ESTCP MM-0601 Demonstration Data Report APG Standardized UXO Test Site**

G.R. HARBAUGH

*Nova Research, Inc.  
Alexandria, Virginia*

J.B. KINGDON

T. FURUYA

T.H. BELL

*SAIC, Inc. - ASAD  
Arlington, Virginia*

D.A. STEINHURST

*Nova Research, Inc.  
Alexandria, Virginia*

January 14, 2010

Approved for public release; distribution is unlimited.

REPORT DOCUMENTATION PAGE				Form Approved OMB No. 0704-0188	
Public reporting burden for this collection of information is estimated to average 1 hour per response, including the time for reviewing instructions, searching existing data sources, gathering and maintaining the data needed, and completing and reviewing this collection of information. Send comments regarding this burden estimate or any other aspect of this collection of information, including suggestions for reducing this burden to Department of Defense, Washington Headquarters Services, Directorate for Information Operations and Reports (0704-0188), 1215 Jefferson Davis Highway, Suite 1204, Arlington, VA 22202-4302. Respondents should be aware that notwithstanding any other provision of law, no person shall be subject to any penalty for failing to comply with a collection of information if it does not display a currently valid OMB control number. <b>PLEASE DO NOT RETURN YOUR FORM TO THE ABOVE ADDRESS.</b>					
1. REPORT DATE (DD-MM-YYYY) 14-01-2010		2. REPORT TYPE Interim Report		3. DATES COVERED (From - To) March 26 - August 15, 2008	
4. TITLE AND SUBTITLE  EMI Array for Cued UXO Discrimination ESTCP MM-0601 Demonstration Data Report APG Standardized UXO Test Site				5a. CONTRACT NUMBER	
				5b. GRANT NUMBER	
				5c. PROGRAM ELEMENT NUMBER 0603851D8Z	
6. AUTHOR(S)  G.R. Harbaugh,* J.B. Kingdon,† T. Furuya,† T.H. Bell,† and D.A. Steinhurst*				5d. PROJECT NUMBER MM-0601	
				5e. TASK NUMBER	
				5f. WORK UNIT NUMBER 61-5802-H-9	
7. PERFORMING ORGANIZATION NAME(S) AND ADDRESS(ES)  Naval Research Laboratory, Code 6110 4555 Overlook Avenue, SW Washington, DC 20375-5320				8. PERFORMING ORGANIZATION REPORT NUMBER  NRL/MR/6110--10-9234	
9. SPONSORING / MONITORING AGENCY NAME(S) AND ADDRESS(ES)  Environmental Security Technology Certification Program (ESTCP) Program Office 901 North Stuart Street, Suite 303 Arlington, VA 22203				10. SPONSOR / MONITOR'S ACRONYM(S) ESTCP	
				11. SPONSOR / MONITOR'S REPORT NUMBER(S)	
12. DISTRIBUTION / AVAILABILITY STATEMENT  Approved for public release; distribution is unlimited.					
13. SUPPLEMENTARY NOTES *Nova Research, Inc., 1900 Elkin Street, Suite 230, Alexandria, VA 22308 †SAIC, Inc. - ASAD, 1225 South Clark Street, Suite 800, Arlington, VA 22202					
14. ABSTRACT  A new time-domain EMI sensor for the purpose of UXO classification under ESTCP project MM-0601 has been constructed and characterized. A vehicle-towed, 2m × 2m array of 25 of these sensors was demonstrated at the Aberdeen Test Center. The array was used as part of a two-step process for identifying and classifying buried metal targets where the anomalies for cued investigation were previously identified with a survey system. The resultant data (625 bi-static pairs) therefore have near-perfect spatial correlation and no motion-induced noise. The performance of the sytem is evaluated in terms of the performance metrics established in the demonstration plan, in part using the recently published ATC scoring report.					
15. SUBJECT TERMS Discrimination      Unexploded Ordnance (UXO)      Electromagnetic Induction (EMI) Classification      Multi-sensor Towed Array Detection System (MTADS)      Magnetometry					
16. SECURITY CLASSIFICATION OF:			17. LIMITATION OF ABSTRACT  UL	18. NUMBER OF PAGES  76	19a. NAME OF RESPONSIBLE PERSON B.J. Spargo, NRL, Code 6110
a. REPORT Unclassified	b. ABSTRACT Unclassified	c. THIS PAGE Unclassified			19b. TELEPHONE NUMBER (include area code) (202) 404-6392

## Contents

Figures.....	viii
Tables.....	xi
Acronyms.....	xii
1.0 Introduction.....	1
1.1 Background.....	1
1.2 Objective of the Demonstration.....	1
1.3 Regulatory Drivers.....	1
2.0 Technology .....	2
2.1 Technology Description.....	2
2.1.1 EMI Sensors.....	2
2.1.2 Sensor Array .....	5
2.1.3 Application of the Technology .....	9
2.2 Advantages and Limitations of the Technology .....	9
3.0 Performance Objectives .....	11
3.1 Objective: Reduction of False Alarms.....	11
3.1.1 Metric.....	12
3.1.2 Data Requirements.....	12
3.1.3 Success Criteria.....	12
3.2 Objective: Location Accuracy .....	12
3.2.1 Metric.....	12
3.2.2 Data Requirements.....	12
3.2.3 Success Criteria.....	12
3.3 Objective: Production Rate .....	12

3.3.1	Metric .....	13
3.3.2	Data Requirements.....	13
3.3.3	Success Criteria.....	13
3.4	Objective: Analysis Time .....	13
3.4.1	Metric .....	13
3.4.2	Data Requirements.....	13
3.4.3	Success Criteria.....	13
3.5	Objective: Ease of Use.....	13
3.5.1	Data Requirements.....	13
4.0	Site Description.....	14
4.1	Site Selection .....	14
4.2	Site History .....	14
4.3	Site Topography and Geology .....	14
4.4	Munitions Contamination .....	14
4.5	Site Geodetic Control Information.....	15
4.6	Site Configuration.....	15
5.0	Test Design .....	17
5.1	Conceptual Experimental Design .....	17
5.2	Site Preparation.....	18
5.3	Systems Specification .....	18
5.3.1	MTADS Tow Vehicle.....	18
5.3.2	RTK GPS System .....	19
5.3.3	Magnetometer Array .....	20
5.3.4	Time-Domain Electromagnetic Sensor.....	20

5.4	Calibration Activities .....	20
5.5	Data Collection Procedures.....	26
5.5.1	Scale of Demonstration.....	26
5.5.2	Sample Density .....	26
5.5.3	Quality Checks.....	26
5.5.4	Data Handling .....	31
5.5.5	Magnetometer Survey Data Summary .....	31
5.5.6	Calibration Area.....	32
5.5.7	Blind Grid .....	33
5.5.8	Indirect Fire Area Response Curves .....	35
5.5.9	Indirect Fire Area.....	37
5.5.10	Discrimination Survey Data Summary .....	38
5.5.11	Calibration Area.....	39
5.5.12	Blind Grid .....	39
5.5.13	Indirect Fire Area.....	39
5.5.14	Indirect Fire Area Survey Patterns.....	39
5.6	Validation.....	43
6.0	Data Analysis Plan.....	43
6.1	Preprocessing .....	43
6.2	Target Selection for Detection.....	44
6.3	Parameter Estimation .....	45
6.4	Training.....	47
6.5	Classification.....	48
6.6	Data Product Specification .....	48

7.0	Performance Assessment .....	50
7.1	Objective: Reduction of False Alarms .....	51
7.1.1	Metric .....	51
7.1.2	Data Requirements .....	52
7.1.3	Success Criteria .....	52
7.1.4	Results .....	52
7.2	Objective: Location Accuracy .....	54
7.2.1	Metric .....	54
7.2.2	Data Requirements .....	54
7.2.3	Success Criteria .....	54
7.2.4	Results .....	54
7.3	Objective: Production Rate .....	55
7.3.1	Metric .....	55
7.3.2	Data Requirements .....	55
7.3.3	Success Criteria .....	55
7.3.4	Results .....	55
7.4	Objective: Analysis Time .....	56
7.4.1	Metric .....	56
7.4.2	Data Requirements .....	56
7.4.3	Success Criteria .....	56
7.4.4	Results .....	56
7.5	Objective: Ease of Use .....	56
7.5.1	Data Requirements .....	56
7.5.2	Results .....	57

8.0	Schedule of Activities .....	57
9.0	Management and Staffing .....	58
10.0	References .....	59
Appendix A: Points of Contact .....		A-1
Appendix B: Data Formats .....		B-1

## Figures

Figure 2-1 – Construction details of an individual EMI sensor (left panel) and the assembled sensor with end caps attached (right panel). .....	2
Figure 2-2 – Measured transmit current (upper panel), full measured signal decay (middle panel), and gated decay (lower panel) as discussed in the text.....	3
Figure 2-3 – Measured response from a 2-in steel sphere 25 cm from the sensor. Decays 1, 1001, 2001, and 3001 from a series that started from a cold start are plotted along with the expected response from this target.....	4
Figure 2-4 – Measured response from three calibration coils and the background response between measurements plotted on a semi-log plot to emphasize the exponential nature of the decay. The decay time constants extracted from the measurements are listed in the legend.....	4
Figure 2-5 – Sketch of the EMI sensor array showing the position of the 25 sensors and the three GPS antennae. ....	5
Figure 2-6 – Sensor array mounted on the MTADS EMI sensor platform. ....	5
Figure 2-7 – Comparison of the response of the array members. The measured decay from a 2-in steel sphere held 30 cm below each sensor in turn is plotted. The decays are indistinguishable. ....	6
Figure 2-8 – The response of nine of the individual sensors to a 40-mm projectile located under the center of the array. ....	7
Figure 2-9 – Derived response coefficients for a 40-mm projectile using the measurements of which the decays shown in Figure 2-8 are a subset.....	8
Figure 2-10 – Derived response coefficients from a cued measurement over "Cylinder E" in the test field.....	8
Figure 2-11 – Three sets of $\beta$ s derived from three measurements over a 4.2-in mortar baseplate at different position/orientation pairs.....	9
Figure 4-1 – Map of the reconfigured APG Standardized UXO Test Site. ....	16
Figure 5-1 – Schedule of Field Testing Activities. ....	18
Figure 5-2 – MTADS tow vehicle and magnetometer array. ....	19



Figure 5-3 – Average polarizability for all measurements at APG of the 4” Aluminum sphere as a function of decay time .....	21
Figure 5-4 – Comparison of measured (blue) versus theoretical (red) polarizability as a function of time for the 4” Aluminum sphere.....	22
Figure 5-5 – Comparison of measured (blue) versus library (red) polarizability as a function of time for Calibration Area item H1, 60mm Mortar .....	23
Figure 5-6 – Comparison of measured (blue) versus library (red) polarizability as a function of time for Calibration Area item I6, 81mm Mortar.....	23
Figure 5-7 – Comparison of measured (blue) versus library (red) polarizability as a function of time for Calibration Area item K3, 105mm Projectile.....	24
Figure 5-8 – Discrimination Array background measurement locations. The boundaries of the ATC test field areas are shown for reference. ....	25
Figure 5-9 – Monostatic QC contour plot for Calibration Area item I6 .....	28
Figure 5-10 – Polarizability as a function of time for a 105mm HEAT Projectile with all data included. The fit coherence for all elements included was 0.699. ....	28
Figure 5-11 – Polarizability as a function of time for a 105mm HEAT Projectile with element 21 excluded. The fit coherence with element 21 excluded was 0.992.....	29
Figure 5-12 – Monostatic QC contour plot for example anomaly .....	30
Figure 5-13 - Polarizability as a function of time for the example show in Figure 5-12 with all data included. The fit coherence for all elements included was 0.652.....	30
Figure 5-14 - Polarizability as a function of time for the example show in Figure 5-12 with elements 0,5,10,11,15,16,17,20,21,22 excluded. The fit coherence for the remaining elements was 0.985. ....	31
Figure 5-15 – Magnetometer anomaly map for the APG Calibration Area. ....	33
Figure 5-16 – Magnetometer system coverage map for the APG Blind Grid. ....	34
Figure 5-17 – Magnetometer response curve for the ATC standard 60mm Mortar .....	35
Figure 5-18 – Magnetometer response curve for the ATC standard 81mm Mortar .....	36
Figure 5-19 – Magnetometer response curve for the ATC standard 105mm Projectile .....	36

Figure 5-20 – Magnetometer system coverage map for the APG Indirect Fire Area.....	38
Figure 5-21 – A portion of the Indirect Fire Area with anomaly locations flagged. ....	40
Figure 5-22 – A portion of the Indirect Fire Area with anomalies binned into 2-m swaths. The anomalies are shown in black, the planed route is shown in red. ....	41
Figure 5-23 – A portion of the Indirect Fire Area with anomalies binned into 1-m swaths. The anomalies are shown in black, the planed route is shown in red. ....	42
Figure 6-1 – Principal axis polarizabilities for a ½ cm thick by 25cm long by 15cm wide mortar fragment. ....	46
Figure 6-2 – Accuracy of depth estimates from TEM array ( $1\sigma = 6.1$ cm) compared to MTADS magnetometer array ( $1\sigma = 5.4$ cm) .....	47
Figure 6-3 – Reporting Template for APG Blind Grid.....	49
Figure 6-4 – Reporting Template for APG Indirect Fire Area. ....	49
Figure 8-1 – Schedule for all demonstration activities including deliverables.....	57
Figure 9-1 – Demonstration management and staffing diagram. ....	58

## Tables

Table 3-1 – Performance Objectives for This Demonstration .....	11
Table 4-1 – Geodetic Control at the APG Demonstration Site.....	15
Table 5-1 – Discrimination Array background measurement locations .....	26
Table 5-2 – Ranking categories for IDF magnetometer anomalies and number of anomalies in each category .....	37
Table 7-1 – Performance Results for This Demonstration .....	51
Table 7-2 – TEMTADS Blind Grid Test Area $P_d^{disc}$ Results.....	52
Table 7-3 – TEMTADS Blind Grid Test Area $P_{fp}^{disc}$ Results.....	52
Table 7-4 – TEMTADS Indirect Fire Test Area $P_d^{disc}$ Results .....	53
Table 7-5 – TEMTADS Indirect Fire Test Area $P_{fp}^{disc}$ Results .....	53
Table 7-6 – TEMTADS Blind Grid Test Area Efficiency and Rejection Rates.....	53
Table 7-7 – TEMTADS Indirect Fire Test Area Efficiency and Rejection Rates .....	54
Table 7-8 – TEMTADS Blind Grid Test Area Location Error and Standard Deviation.....	55
Table 7-9 – TEMTADS Indirect Fire Test Area Location Error and Standard Deviation .....	55

## Acronyms

AOL	Advanced Ordnance Locator
APG	Aberdeen Proving Ground
ATC	Aberdeen Test Center
DAQ	Data Acquisition Computer
DAS	Data Analysis System
EMI	Electromagnetic Induction
GIS	Geographic Information System
GPS	Global Positioning System
MTADS	Multi-sensor Towed Array Detection System
NMEA	National Marine Electronics Association
NRL	Naval Research Laboratory
POC	Point of Contact
(PTNL,)AVR	Time, Yaw, Tilt Range NMEA-0183 sentence
(PTNL,)GGK	Time, Position, Fix Quality, PDOP NMEA-0183 sentence
RTK	Real-time Kinematic
Rx	Receive
SNR	Signal-to-Noise Ratio
TEM	Time-domain Electromagnetic Induction
Tx	Transmit
UTC	Universal Time Coordinated
UXO	Unexploded Ordnance

## **1.0 INTRODUCTION**

### **1.1 BACKGROUND**

Unexploded Ordnance (UXO) detection and remediation is a high priority triservice requirement. As the Defense Science Board recently wrote: “Today’s UXO cleanup problem is massive in scale with some 10 million acres of land involved. Estimated cleanup costs are uncertain but are clearly tens of billions of dollars. This cost is driven by the digging of holes in which no UXOs are present. The instruments used to detect UXOs (generally located underground) produce many false alarms, - i.e., detections from scrap metal or other foreign or natural objects - , for every detection of a real unexploded munition found.” [1]

There is general agreement that the best solution to the false alarm problem involves the use of EMI sensors which, in principle, allow the extraction of target shape parameters in addition to a size and depth estimate. We, and others, have fielded systems with either time-domain or frequency-domain EMI sensors with the goal of extracting reliable target shape parameters and, thus, improving the discrimination capability of our surveys. In practice, the discrimination ability of these sensors has been limited by signal-to-noise limitations. Three of the largest noise terms are inherent sensor noise, motion-induced noise, and sensor location uncertainty.

The three most successful demonstrations of EMI-based discrimination all involved cued detection with gridded collection of EMI data [2-4]. The success of the gridded data collections was due to the combination of minimal location uncertainty, no motion-induced noise, and sufficient SNR. The downside of the implementations previously demonstrated is that they were relatively slow and inefficient, especially on a large site. We have constructed an EMI sensor array that combines the classification ability of a gridded survey with the coverage efficiency of a vehicular array. By coming to a stop over each target to be investigated we are able to obtain all the benefits of a gridded survey (negligible relative sensor location uncertainty, no motion-induced noise, and high SNR) while moving rapidly to the next target with no set-up required gives us the coverage efficiency required for practical success.

### **1.2 OBJECTIVE OF THE DEMONSTRATION**

The objective of this demonstration was to validate the technology through a blind test at one of the Standardized UXO Test Sites. We have previously done a shake-down demonstration of the technology at our Blossom Point, MD field site but a blind test is the only true measure of system performance.

### **1.3 REGULATORY DRIVERS**

Stakeholder acceptance of the use of discrimination techniques on real sites will require demonstration that these techniques can be deployed efficiently and with high probability of discrimination. The first step in this process is to demonstrate acceptable performance on a test site such as that at Aberdeen. After that hurdle has been passed, successful demonstration at a live site will facilitate regulatory acceptance of the methods.

## 2.0 TECHNOLOGY

### 2.1 TECHNOLOGY DESCRIPTION

#### 2.1.1 EMI Sensors

The EMI sensor used in the Discrimination Array is based on the Navy-funded Advanced Ordnance Locator (AOL), developed by G & G Sciences. The AOL consists of three transmit coils arranged in a 1-m cube; we have adopted the transmit (Tx) and receive (Rx) subsystems of this sensor directly, converted to a 5 x 5 array of 35 cm sensors, and made minor modifications to the control and data acquisition computer to make it compatible with our deployment scheme.

A photograph of an individual sensor element under construction is shown in the left panel of Figure 2-1. The transmit coil is wound around the outer portion of the form and is 35 cm on a side. The 25-cm receive coil is wound around the inner part of the form which is re-inserted into the outer portion. An assembled sensor with the top and bottom caps used to locate the sensor in the array is shown in the right panel of Figure 2-1.

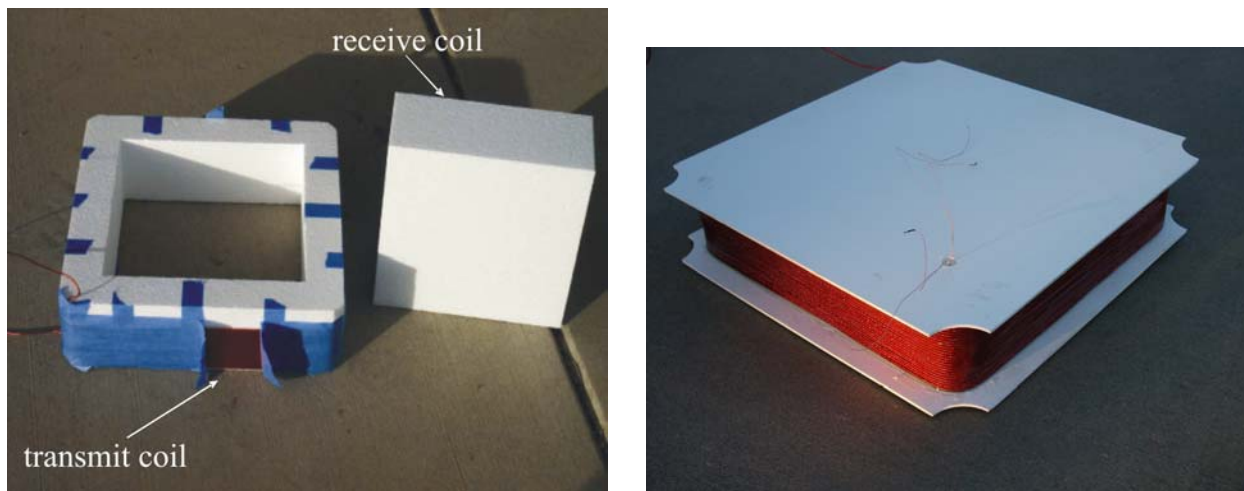


Figure 2-1 – Construction details of an individual EMI sensor (left panel) and the assembled sensor with end caps attached (right panel).

Decay data are collected with a 500 kHz sample rate until 25ms after turn off of the excitation pulse. This results in a raw decay of 12,500 points; too many to be practical. These raw decay measurements are grouped into 115 logarithmically-spaced “gates” whose center times range from 42  $\mu$ s to 24.35 ms with 5% widths and are saved to disk. An example of the measured transmit pulse, raw decay, and gated decay is shown in Figure 2-2.

The individual sensors (consisting of transmit electronics, transmit and receive coils, pre-amp, and digitizer) were characterized at G & G Sciences before approval was given for construction of the array. Examples of the characterization data are shown in Figure 2-3 and Figure 2-4.

System stability is shown in Figure 2-3 which plots the normalized (by measured transmit current) response of a 2 in steel ball at 25 cm separation from the sensor. The data plotted are decays 1, 1001, 2001, and 3001 in a continuously-triggered series that began from a cold start and ran for 150 minutes. For comparison purposes, the expected response from this sphere is plotted in black. As can be seen, the sensor exhibits excellent stability which will be important for the cued deployment planned.

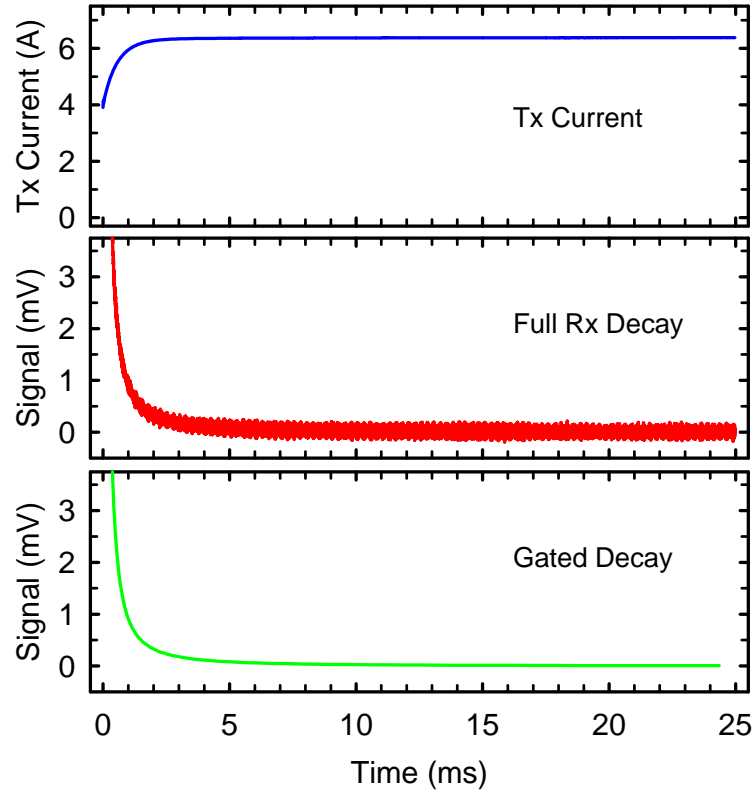


Figure 2-2 – Measured transmit current (upper panel), full measured signal decay (middle panel), and gated decay (lower panel) as discussed in the text.

The second important characterization test is sensor response linearity. Since we plan to collect decay data to late times and over several orders of magnitude in amplitude, the linearity of system response is very important. To characterize this property of the sensor, we constructed a series of copper coils with nominal decay time constants of 2, 4, and 6 ms. The response of the three coils is shown in Figure 2-4 which plots the measured decay on a semi-log axes. After a transient at early times, the decays exhibit clean exponential behavior with measured decay times of 1.8, 3.3, and 5.8 ms. Careful calculation of the expected decay times at the temperature at which the tests were conducted results in expected values of 1.82, 3.26, and 5.73 ms; the measured values are in excellent agreement with these.

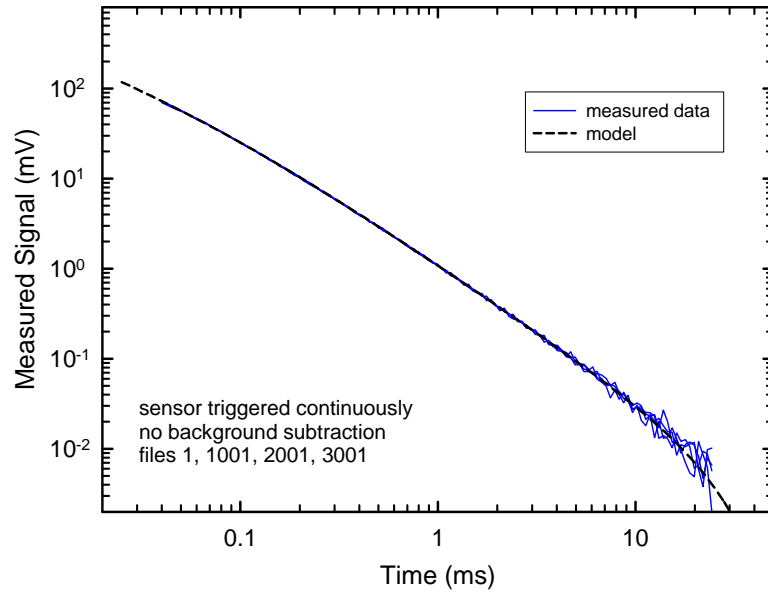


Figure 2-3 – Measured response from a 2-in steel sphere 25 cm from the sensor. Decays 1, 1001, 2001, and 3001 from a series that started from a cold start are plotted along with the expected response from this target.

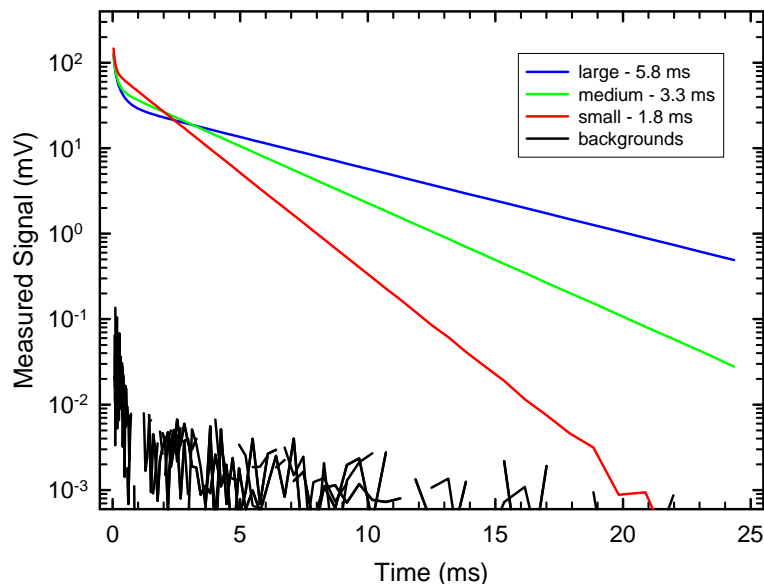


Figure 2-4 – Measured response from three calibration coils and the background response between measurements plotted on a semi-log plot to emphasize the exponential nature of the decay. The decay time constants extracted from the measurements are listed in the legend.



### 2.1.2 Sensor Array

The twenty-five individual sensors are arranged in a 5 x 5 array as shown in Figure 2-5. The center-to-center distance is 40 cm yielding a 2 m x 2 m array. Also shown in Figure 2-5 is the position of the three GPS antennae that are used to determine the location and orientation of the array for each cued measurement. A picture of the array mounted on the MTADS EMI sensor platform is shown in Figure 2-6.

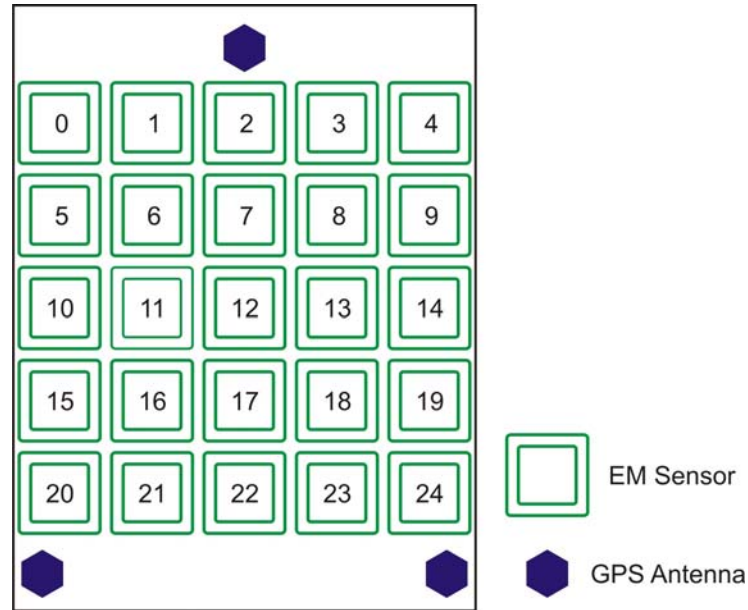


Figure 2-5 – Sketch of the EMI sensor array showing the position of the 25 sensors and the three GPS antennae.



Figure 2-6 – Sensor array mounted on the MTADS EMI sensor platform.

After assembly of the array, a number of array calibration measurements were performed. The first task was to ensure that each of the individual sensors has equivalent response. A jig was constructed that allows us to mount a 2-in steel sphere 30 cm below each array element in turn. Data collected using this jig are shown in Figure 2-7. As can be seen, the measured decays from each of the sensors plotted are indistinguishable.

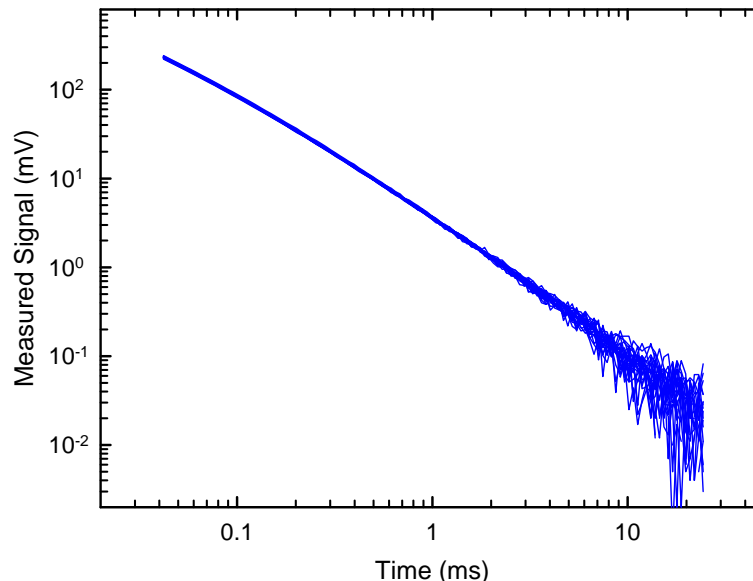


Figure 2-7 – Comparison of the response of the array members. The measured decay from a 2-in steel sphere held 30 cm below each sensor in turn is plotted. The decays are indistinguishable.

After this, the assembled array was used to measure the response of a number of inert ordnance items and stimulants mounted on a test stand, placed in our test pit, or buried in our test field. For each series of measurements with the full array, we cycle through the sensors transmitting from each in turn. After each excitation pulse, we record the response of all twenty-five receive coils. Thus, there are 625 (25 x 25) individual transmit/receive pairs recorded, making it difficult to present a full measurement in any coherent way. In Figure 2-8, we plot nine of the transmit/receive pairs resulting from excitation of a 40-mm projectile located under the center of the array. The decays plotted correspond to the signal received on the nine central sensors (reference Figure 2-5 for the sensor numbering) when that sensor transmits. In other words, the results of nine individual monostatic measurements are presented.

All 625 measurements are used for the inversion to recover target parameters. The inversion results for the decay data shown in Figure 2-8 are shown in Figure 2-9. As we expect for an object with axial symmetry such as a 40-mm projectile, we recover one large response coefficient and two equal, but smaller ones. These response coefficients will be the basis of the discrimination decisions in this demonstration. Derived  $\beta$ s for “Cylinder E” (3" x 12" steel cylinder) in the test field are shown for comparison in Figure 2-10.

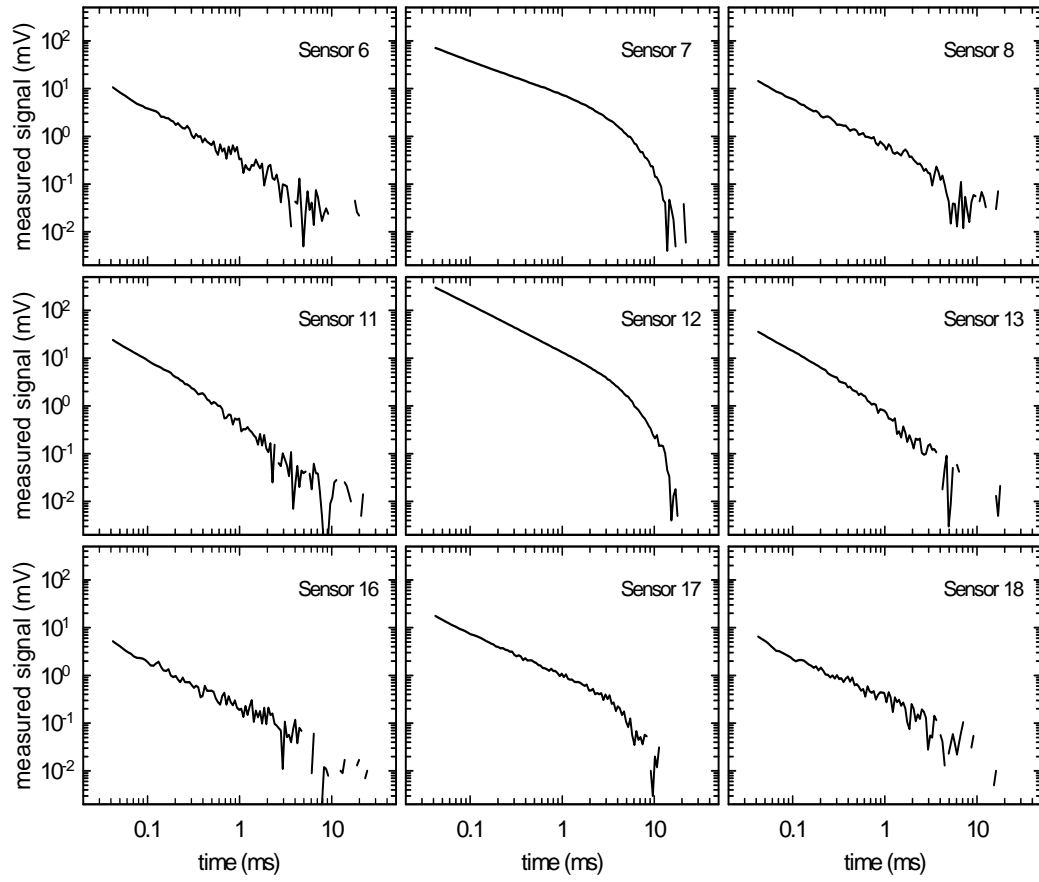


Figure 2-8 – The response of nine of the individual sensors to a 40-mm projectile located under the center of the array.

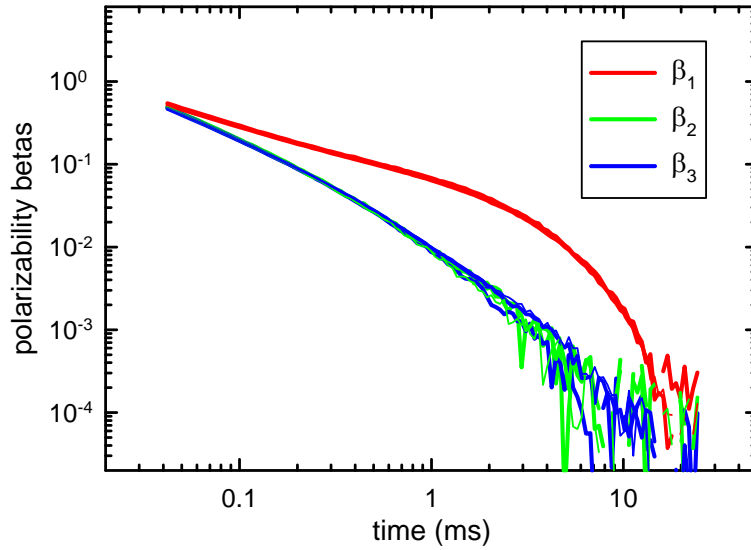


Figure 2-9 – Derived response coefficients for a 40-mm projectile using the measurements of which the decays shown in Figure 2-8 are a subset.

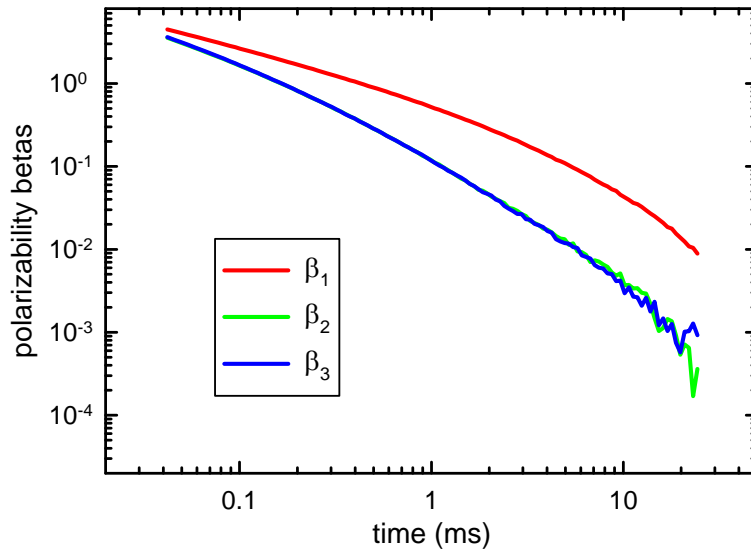


Figure 2-10 – Derived response coefficients from a cued measurement over "Cylinder E" in the test field.

The final array characterization test was to confirm that the response coefficients we recover are invariant to object position and orientation under the array. Figure 2-11 shows the derived  $\beta$ s plotted for a 4.2-in mortar baseplate after measurements at three position/orientation pairs. As can be seen, the inversion results are robust to variation in the object's position and orientation.

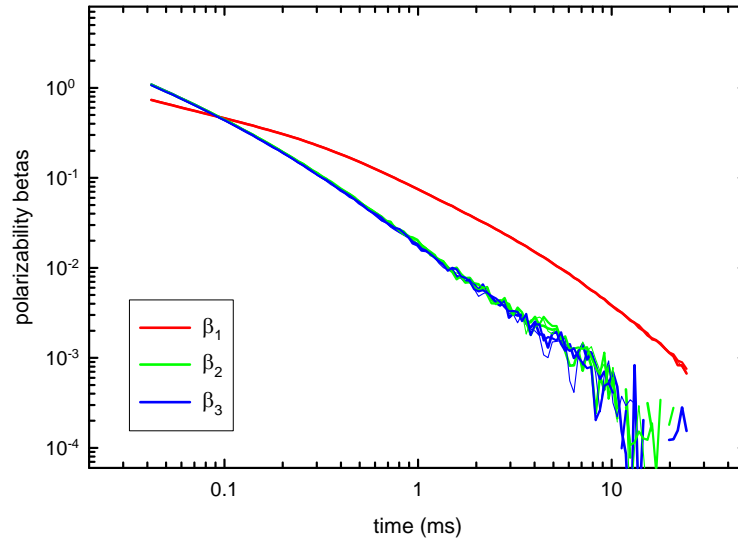


Figure 2-11 – Three sets of  $\beta$ s derived from three measurements over a 4.2-in mortar baseplate at different position/orientation pairs.

### 2.1.3 Application of the Technology

Application of this technology is straightforward. A list of target positions is developed from a survey by some geophysical instrument; in the case of this demonstration, the MTADS magnetometer array. This target file, containing the target location and an optional flag for additional ‘stacking’ or averaging, is transferred to the system control program which uses the information from the three GPS antennae to guide the operator to position the array over each target in turn. When positioned over the target, the data acquisition computer steps through the array sensors sequentially, just as in the characterization measurements discussed in the preceding section, and collects decays from all twenty-five receive coils for each excitation. These data are then inverted for target location and characteristics. At the end of the EMI data collection, a few seconds of platform position and orientation data are collected to be used to translate the inverted target position, which is, of course, relative to the array, to absolute position and orientation.

In the final version of this technology, the inversion will be performed while the operator is driving the array to the next target. For this demonstration, we performed the inversions off-line so that we would have the ability to intervene in the automatic process as required. The EMI and position data were transferred to the analyst several times each day for near real-time analysis at the demonstration site.

## 2.2 ADVANTAGES AND LIMITATIONS OF THE TECHNOLOGY

The Discrimination Array is designed to combine the data quality advantages of a gridded survey with the coverage efficiencies of a vehicular system. The design goal of this system is to collect data equal, if not better, in quality to the best gridded surveys (the relative position and

orientation of the sensors being known better than for gridded data) while prosecuting many more targets each field day.

There are obvious limitations to the use of this technology. The array is a 2-m square so fields where the vegetation or topography interferes with passage of a trailer that size will not be amenable to the use of the present array. During the course of this, and subsequent, demonstrations we will be evaluating the utility of a 3 x 3 sub-array of sensors. If we can utilize the sub-array, we can increase the number of sites for which this technology will be appropriate. The other serious limitation will be anomaly density. For all sensors, there is a limiting anomaly density above which the response of individual targets cannot be separated. We have chosen relatively small sensors for this array which should help with this problem but we cannot eliminate it. Based on experiments at our test pit at Blossom Point, the results of this demonstration, and work done on the Camp Sibert data sets, anomaly densities of 300 anomalies/acre or higher would limit the applicability of this system as more than 20% of the anomalies would have another anomaly within a meter.

### 3.0 PERFORMANCE OBJECTIVES

The performance objectives for this demonstration are summarized in Table 3-1. Since the Discrimination Array is a discrimination technology, the performance objectives focus on the second step of the UXO survey problem; we assume that the anomalies from all targets of interest have been detected and included on the target list that we worked from.

Table 3-1 – Performance Objectives for This Demonstration

Performance Objective	Metric	Data Required	Success Criteria
<b>Quantitative Performance Objectives</b>			
Reduction of False Alarms	Number of false alarms eliminated at demonstrator operating point.	<ul style="list-style-type: none"><li>• Prioritized dig list</li><li>• Scoring report from APG</li></ul>	Reduction of false alarms by > 50% with 95% correct identification of munitions
Location Accuracy	Average error and standard deviation in both axes for interrogated items	<ul style="list-style-type: none"><li>• Estimated location from analysis</li><li>• Scoring report from APG</li></ul>	$\Delta N$ and $\Delta E < 10$ cm $\sigma N$ and $\sigma E < 15$ cm
Production Rate	Number of targets interrogated each day	<ul style="list-style-type: none"><li>• Log of field work</li></ul>	75 targets per day
Analysis Time	Average time required for inversion and classification	<ul style="list-style-type: none"><li>• Log of analysis work</li></ul>	15 min per target
<b>Qualitative Performance Objective</b>			
Ease of Use		<ul style="list-style-type: none"><li>• Feedback from operator on ease of use</li></ul>	Operator comes to work smiling

#### 3.1 OBJECTIVE: REDUCTION OF FALSE ALARMS

This is the primary measure of the effectiveness of this technology. By collecting high-quality, precisely-located data, we expect to be able to discriminate munitions from scrap and frag with high efficiency.

### **3.1.1 Metric**

At a seeded test site such as the APG standardized test site, the metric for false alarm elimination is straightforward. We prepared a ranked dig list for the targets we interrogated with a dig/no-dig threshold indicated and ATC personnel used their automated scoring algorithms to assess our results.

### **3.1.2 Data Requirements**

The identification of most of the items in the test field is known to the test site operators. Our ranked dig list is the input for this standard and ATC's standard scoring is the output.

### **3.1.3 Success Criteria**

The objective will be considered to be met if more than 50% of the non-munitions items were labeled as no-dig while retaining 95% of the munitions items on the dig list.

## **3.2 OBJECTIVE: LOCATION ACCURACY**

An important measure of how efficiently any required remediation will proceed is the accuracy of predicted location of the targets marked to be dug. Large location errors lead to confusion among the UXO techs assigned to the remediation costing time and often leading to removal of a small, shallow object when a larger, deeper object was the intended target.

### **3.2.1 Metric**

As above, the metric for location accuracy is straightforward at a seeded test site such as the APG standardized test site. We provided an estimated position for all targets we interrogated and ATC personnel used their automated scoring algorithms to assess our results.

### **3.2.2 Data Requirements**

The location of most of the items in the test field is known to the test site operators. Our dig list is the input for this standard and ATC's standard scoring is the output.

### **3.2.3 Success Criteria**

The objective will be considered to be met if the average position error was less than 10 cm in both dimensions (low bias) and the standard deviation of each dimension was less than 15 cm (accurate location).

## **3.3 OBJECTIVE: PRODUCTION RATE**

Even if the performance of the technology on the two metrics above is satisfactory, there is an economic metric to consider. There is a known cost of remediating a suspected munitions item. If the cost to interrogate a target is greater than this cost, the technology will be useful only at



sites with special conditions or target values. Note, however, that in its ultimate implementation this technology will result in reacquisition, cued interrogation, and target flagging in one visit to the site.

### **3.3.1 Metric**

The number of targets interrogated per day is the metric for this objective. Combined with the daily operating cost of the technology this gives the per-item cost.

### **3.3.2 Data Requirements**

Survey productivity was determined from a review of the ATC demonstration field logs.

### **3.3.3 Success Criteria**

For this first demonstration, the objective will be considered to be met if at least 75 targets were interrogated each survey day.

## **3.4 OBJECTIVE: ANALYSIS TIME**

The ultimate implementation of this technology will involve on-the-fly analysis and classification. The time for this will be limited to the driving time to the next anomaly on the list. We will track the near-real-time analysis time in this demonstration.

### **3.4.1 Metric**

The time required for inversion and classification per anomaly is the metric for this objective

### **3.4.2 Data Requirements**

Analysis time was determined from a review of the data analysis logs.

### **3.4.3 Success Criteria**

For this first demonstration, the objective will be considered to be met if the average inversion and classification time was less than 15 min.

## **3.5 OBJECTIVE: EASE OF USE**

This qualitative objective is intended as a measure of the long-term usability of the technology. If the operator does not report that the technology is easy to use, shortcuts that can compromise the efficiency of the technology will begin to creep into daily operations.

### **3.5.1 Data Requirements**

This objective was evaluated based on operator feedback.

## **4.0 SITE DESCRIPTION**

This demonstration was conducted at the APG Standardized UXO Technology Demonstration Site located at the Aberdeen Proving Ground, MD during the period of May through June, 2008.

### **4.1 SITE SELECTION**

This was our first field demonstration of this combination of EMI sensors and survey mode. As such, the demonstration was conducted on the Standardized UXO Test Site at APG. The APG site is located close to our base of operations in southern Maryland and therefore minimizes the logistics costs of the deployment. Use of this site allows us to receive validation results from near-real-world conditions without incurring the logistics and intrusive investigation expenses that would be required for a demonstration at a live site.

### **4.2 SITE HISTORY**

The Standardized UXO Technology Demonstration Site is adjacent to the Trench Warfare facility at the Aberdeen Proving Ground. The specific area was used for a variety of ordnance tests over the years. Initial magnetometer and EMI surveys conducted by the MTADS team performed after a “mag and flag” survey of the same area identified over a thousand remaining anomalies. These data were used for a final clean up of the site prior to the emplacement of the original test items. Prior to the two subsequent reconfiguration events, unexplained anomalies identified by demonstrators using the site were also investigated and removed.

### **4.3 SITE TOPOGRAPHY AND GEOLOGY**

According to the soils survey conducted for the entire area of APG in 1998, the test site consists primarily of Elkton Series type soil [5]. The Elkton Series consist of very deep, slowly permeable, poorly drained soils. These soils formed in silty aeolin sediments and the underlying loamy alluvial and marine sediments. They are on upland and lowland flats and in depressions of the Mid-Atlantic Coastal Plain. Slopes range from 0 to 2 percent.

Overall, the demonstration site is relatively flat and level. There are some low-lying areas in the northwest portion of the site that tend to have standing water during the wet periods of the year. The current sensor system is not sufficiently weatherproofed to operate through standing water. However, during the most recent reconfiguration, the areas most prone to being underwater were excluded from the survey scenarios. Anomalies that were located underwater or nearby to water at the time of survey were deferred until the end of the survey and were interrogated by carefully, if less efficiently, maneuvering the array into position.

### **4.4 MUNITIONS CONTAMINATION**

The area currently occupied by the Standardized site has seen an extensive history of munitions use. As an example, in 2003 we conducted a magnetometer survey of a previously unremediated area directly adjacent to the Standardized site [6]. In a survey area of approximately 1 hectare,

we identified 2479 anomalies, of which 1921 were amenable to a model fit using our standard analysis. Historical records provided by ATC and previous remediation results indicated that the likely munitions of interest for this site were:

- Grenades, MkI, MkII, and French VB Rifle w/o chute
- Grenades, French VB Rifle w/ chute
- 60mm mortars (including 2" Smoke)
- 3" Stokes (Smoke and HE)
- 105 mm projectiles
- 155 mm projectiles

#### 4.5 SITE GEODETIC CONTROL INFORMATION

There are two first-order points on the site for use as GPS base station points. Their reported coordinates are listed in Table 4-1. The horizontal datum for all values is NAD83. The vertical control is referenced to the NAVD88 datum and the Geoid03 geoid. Point 477 was used as the GPS base station point for the entirety of this demonstration.

Table 4-1 – Geodetic Control at the APG Demonstration Site

ID	Latitude	Longitude	Elevation	Northing	Easting	HAE
477	39° 28' 18.63880" N	76° 07' 47.71815"W	10.669 m	4,369,749.013	402,810.038	-22.545
478	39° 28' 04.24219" N	76° 07' 48.50439"W	11.747 m	4,369,305.416	402,785.686	-21.473

#### 4.6 SITE CONFIGURATION

Figure 4-1 is a map of the Standardized UXO Technology Demonstration Site at APG. The Calibration and Blind Grids are shown along with the various Open Field Areas.

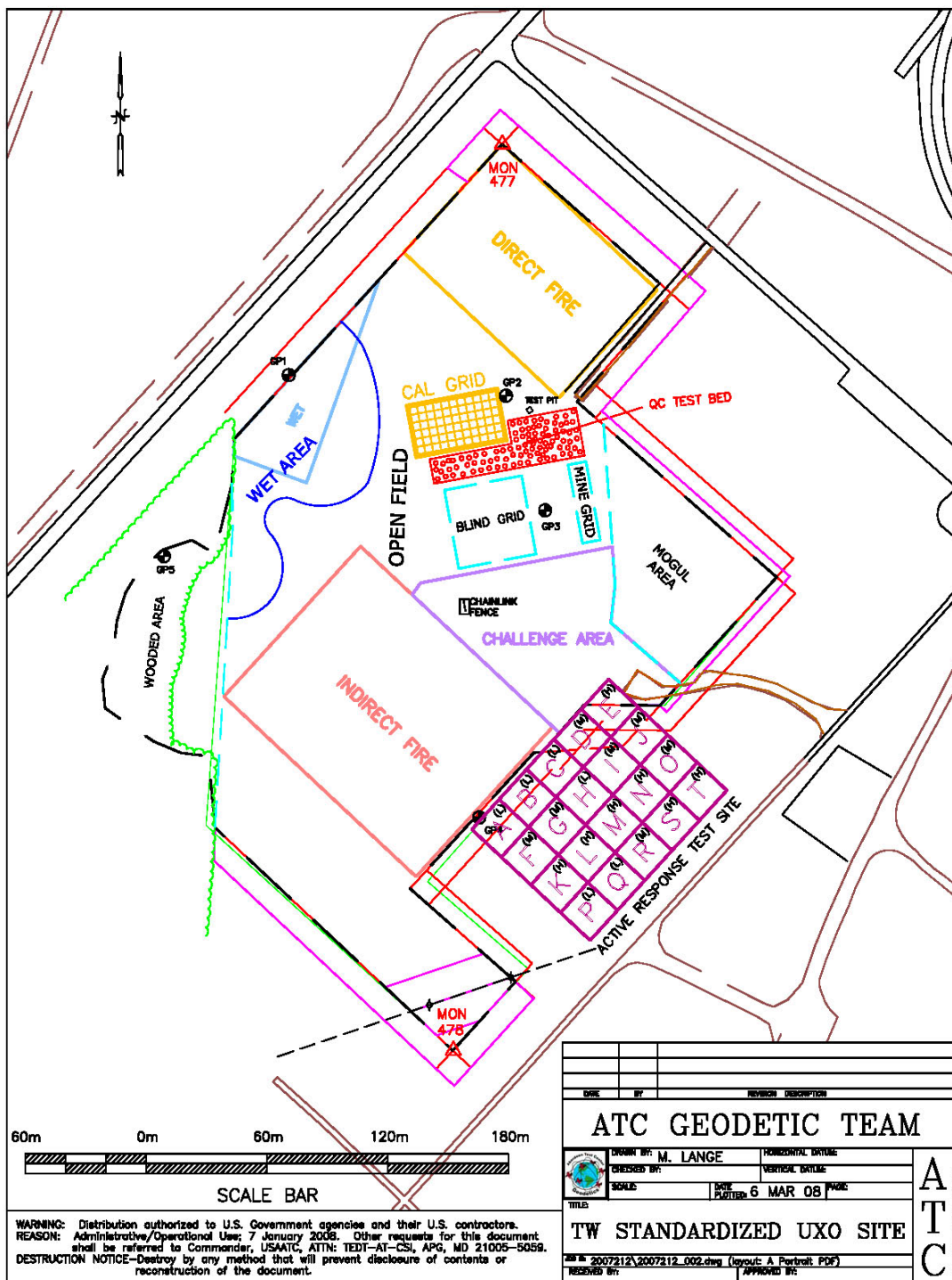


Figure 4-1 – Map of the reconfigured APG Standardized UXO Test Site.

## **5.0 TEST DESIGN**

### **5.1 CONCEPTUAL EXPERIMENTAL DESIGN**

The demonstration was designed to be executed in two stages. The first stage was a standard MTADS magnetometer survey of the Calibration, Blind Grid, and the Indirect Fire Area of the Standardized Site. An experienced data analyst manually inspected the Blind Grid data and made a determination for each cell as to whether or not an anomaly was present. Anomaly locations were identified from the magnetometer data from the Indirect Fire Area in a combination automated / manual method as described in Sections 5.5.9 and 6.2. A data segment around each anomaly center was extracted and analyzed using the UX-Analyze subsystem of the Oasis montaj software package as described in Section 6.2 to fit the data to a dipole model and extract the associated fit parameters (position, depth, equivalent size). These fit results constituted the source anomaly list for the second stage of the demonstration.

In practice, the majority of the site was surveyed as a whole with the magnetometer system and the resulting data were analyzed in parallel to the above effort. The results were provided to the Program Office in support of the recent reconfiguration effort. Anomalies were detected in a manner similar to that used for MTADS data sets collected as part of the ESTCP UXO Discrimination Study at the former Camp Sibert [7].

This method relies on the establishment of an anomaly detection threshold. At the former Camp Sibert demonstration site, a single munitions type was present. Pit measurements at various depths and orientations of an example article were made and bounding response curves generated for the 4.2-in mortar, the munitions of interest. The anomaly detection threshold was then set based on the least-favorably predicted response at the USACoE standard 11x depth. For our recent GEMTADS demonstration at F.E. Warren AFB, two primary munitions types were present, 37 and 75mm projectiles. In this case, response curves were generated for each munitions type and the smaller of the two indicated detection thresholds was selected as the overall threshold. In the reconfigured Standardized Site, several areas have been established with different mixes of emplaced munitions. Individual anomaly detection thresholds were established for each area based on an abbreviated set of pit measurements made at Blossom Point for each of the emplaced items. For each area, the smallest appropriate least-favorable response will be used to determine the threshold. A safety factor of 25% was also applied.

As was shown during the ESTCP Project 200413 “Gold Standard” surveys, the dynamic background signal level for the Standardized Test Site at APG was at least 2.5 nT for the magnetometer system. The dynamic background level at the reconfigured site was characterized prior to anomaly selection.

Individual extracted anomalies were analyzed using UX-Analyze. We were able to survey a large majority of the entire site excluding the Wooded and Mogul Areas. At the time of the demonstration, the Challenge Area was unpopulated and was also not surveyed.

The second stage of the demonstration was a survey of the Calibration, Blind Grid, and the Indirect Fire Area using the MTADS Discrimination Array developed as part of ESTCP Project MM-0601. The array was positioned roughly over the center of each anomaly on the source anomaly list and a data set collected. Each data set was then inverted using the data analysis methodology discussed in Section 6.0, estimated target parameters determined, and ultimately a classification made for each cell in the Blind Grid determined to contain an anomaly and each anomaly placed on the Indirect Fire Area anomaly list. The results were then submitted to the Aberdeen Test Center for performance assessment.

The schedule of field testing activities is provided in Figure 5-1 as a Gantt chart.




	Activity Name	May 2008				Jun 2008			
		4	11	18	25	1	8	15	22
1	APG Demonstration								
2	Magnetometer Data Collection								
3	Discrimination Data Collection								
		4	11	18	25	1	8	15	22

Figure 5-1 – Schedule of Field Testing Activities.

## 5.2 SITE PREPARATION

The Standardized UXO Test Sites are configured with clearly-marked calibration, blind validation, and open field scenarios. Several GPS control points are provided at each site. Basic facilities such as portable toilets and field buildings are also provided. Secure storage for larger vehicles and sensor arrays is limited at the APG Test Site. A 40-foot shipping container was mobilized to the site for the duration of the Discrimination Array portion of the demonstration to provide convenient, secure storage for the MTADS tow vehicle and the sensor trailer. The container was removed at the end of the demonstration.

## 5.3 SYSTEMS SPECIFICATION

This demonstration was conducted using the NRL MTADS tow vehicle and subsystems. The tow vehicle and each subsystem are described further in the following sections.

### 5.3.1 MTADS Tow Vehicle

The MTADS has been developed with support from ESTCP. The MTADS hardware consists of a low-magnetic-signature vehicle that is used to tow the different sensor arrays over large areas (10 - 25 acres / day) to detect buried UXO. The MTADS tow vehicle and magnetometer array are shown in Figure 5-2.



Figure 5-2 – MTADS tow vehicle and magnetometer array.

### 5.3.2 RTK GPS System

Positioning is provided using cm-level Real Time Kinematic (RTK) Global Positioning System (GPS) receivers. To achieve cm-level precision, a fixed reference base station is placed on an established first-order survey control point near the survey area. The base station transmits corrections to the GPS rover at 1 Hz via a radio link (450 MHz). For the magnetometer array, a single GPS antenna placed directly above the center of the sensor array is used to measure the sensor positions in real-time (5 Hz) using a vendor-specific NMEA-0183 message format (PTNL,GGK or G GK).

The Discrimination Array is located in three-dimensional space using a three-receiver RTK GPS system shown schematically in Figure 2-5 [8]. The three-receiver configuration extends the concept of RTK operations from that of a fixed base station and a moving rover to moving base stations and moving rovers. The lead GPS antenna (and receiver, Main) receives corrections from the fixed base station at 1 Hz in the same manner as for the magnetometer MTADS. This corrected position is reported at 10-20 Hz. The Main receiver also operates as a ‘moving base,’ transmitting corrections (by serial cable) to the next GPS receiver (AVR1) which uses the corrections to operate in RTK mode.

A vector (AVR1, heading (yaw), angle (pitch), and range) between the two antennae is reported at 10 Hz using a vendor-specific NMEA-0183 message format (PTNL,AVR or AVR). AVR1 also provides ‘moving base’ corrections to the third GPS antenna (AVR2) and a second vector (AVR2) is reported at 10 Hz. All GPS measurements are recorded at full RTK precision, ~2-5 cm. For survey-mode arrays, all sensor readings are typically referenced to the GPS 1-PPS pulse output to fully take advantage of the precision of the GPS measurements. In this case of a cued survey, it is not necessary to address these timing issues. For the cued-mode survey, the GPS position is averaged for 2 seconds as part of the data acquisition cycle. The averaged position and orientation information are then recorded to the position (.gps, ASCII format) data file. The details of the file format are provided in Appendix B.

### 5.3.3 Magnetometer Array

The MTADS magnetometer array is a linear array of eight Cs-vapor magnetometer sensors (Geometrics, Inc., G-822ROV/A). The sensors are sampled at 50 Hz and typical surveys are conducted at 3 m/s. This results in a sampling density of ~6 cm down track with a cross-track sensor spacing of 25 cm. The sensors are nominally mounted 30 cm above the ground. The sensor boom is designed to pivot up to protect the sensors from damage due to impact with obstructions. This degree of freedom allows some variation in sensor height due to surface roughness. Each magnetometer measures the local magnetic field of the earth at the sensor.

A single GPS antenna placed directly above the center of the sensor array is used to measure the sensor positions in real-time (5 Hz). All navigation and sensor data are time-stamped with Universal Coordinated Time (UTC) derived from the satellite clocks and recorded by the data acquisition computer (DAQ) in the tow vehicle. The DAQ runs the MagLogNT software package (v2.921b, Geometrics, Inc.) and the data streams from each device are recorded in separate files with a common root filename.

### 5.3.4 Time-Domain Electromagnetic Sensor

The Discrimination Array is a 5 x 5 square array of individual sensors. Each sensor has dimensions of 40 cm x 40 cm, for an array of 2 m x 2 m overall dimensions. The rationale of this array design is discussed in Reference 9. The result is a cross-track and down-track separation of 40 cm. Sensor numbering is indicated in Figure 2-5. The transmitter electronics and the data acquisition computer are mounted in the tow vehicle. Custom software written by NRL provides both navigation to the individual anomalies and data acquisition functionality. After the array is positioned roughly centered over the center of the anomaly, the data acquisition cycle is initiated. Each transmitter is fired in a sequence winding outward from the center position (12) in a clockwise direction. The received signal is recorded for all 25 Rx coils for each transmit cycle. The transmit pulse waveform duration is 2.7s (0.9s block time, 9 repeats within a block, 3 blocks stacked, with a 50% duty cycle). While it is possible to record the entire decay transient at 500 MHz, we have found that binning the data into 115 time gates simplifies the analysis and provides additional signal averaging without significant loss of temporal resolution in the transient decays [10]. The data are recorded in a binary format as a single file with 25 data points (one data point per Tx cycle). The filename corresponds to the anomaly under investigation.

## 5.4 CALIBRATION ACTIVITIES

For the magnetometer array data collection, no specific calibration activities beyond the standard operational checks<sup>1</sup> were conducted as this is a mature, well-understood technology.

---

<sup>1</sup> See Reference 7 for a discussion of our standard startup operational check procedures.



For the Discrimination Array, a significant amount of data has been collected with the system as configured at our Blossom Point facility, both on a test stand and in the towed configuration on our test field [11]. These data and the corresponding fit parameters provide us with a set of reference parameters including those of clear background (i.e. no anomaly present).

Daily calibration efforts consist of collecting background (no anomaly) data sets at the beginning and end of each survey day and periodically throughout the day at quiet spots as identified from the magnetometer survey to determine the system noise floor. A canonical reference object, a 4" Al sphere, was placed in the test pit located near the Calibration Area and measured each day to monitor the daily variation in the system response. These two types of measurements constituted the daily calibration activities.

The sphere measurements are background subtracted and inverted to obtain the target polarizabilities. These data allow us to calibrate our sensor response in two separate ways. First, by comparing the polarizabilities derived from each separate measurement, we can monitor the daily variation in the system response. In Figure 5-3, we plot the average polarizability for all sphere measurements obtained during our entire run as a function of decay time. Variations of less than 10% of the reference values were observed over the course of eight days.

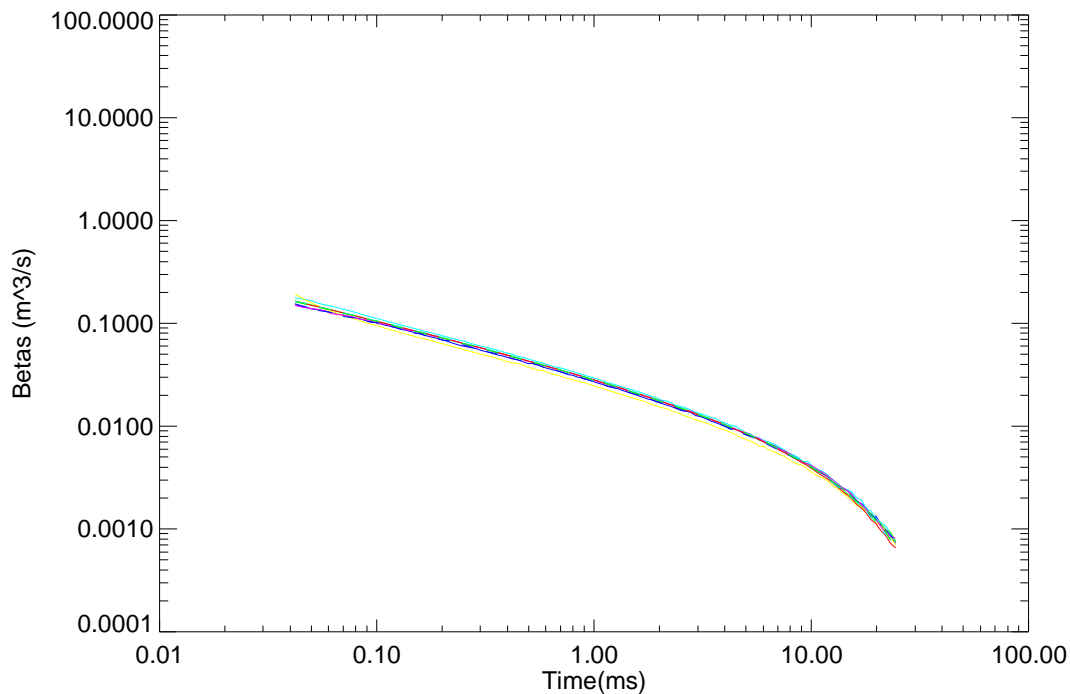


Figure 5-3 – Average polarizability for all measurements at APG of the 4" Aluminum sphere as a function of decay time

Second, we compared our derived polarizabilities directly with the predicted decay of the sphere. The theoretical decay depends on the target's size and conductivity. We have determined this latter value for the sphere by careful measurements with a host of sensors over the years. The

theoretical decay is then calculated and the derived polarizabilities are scaled in amplitude to produce the best match. Figure 5-4 shows the result for one measurement. All daily calibration data sets are included on the accompanying DVD.

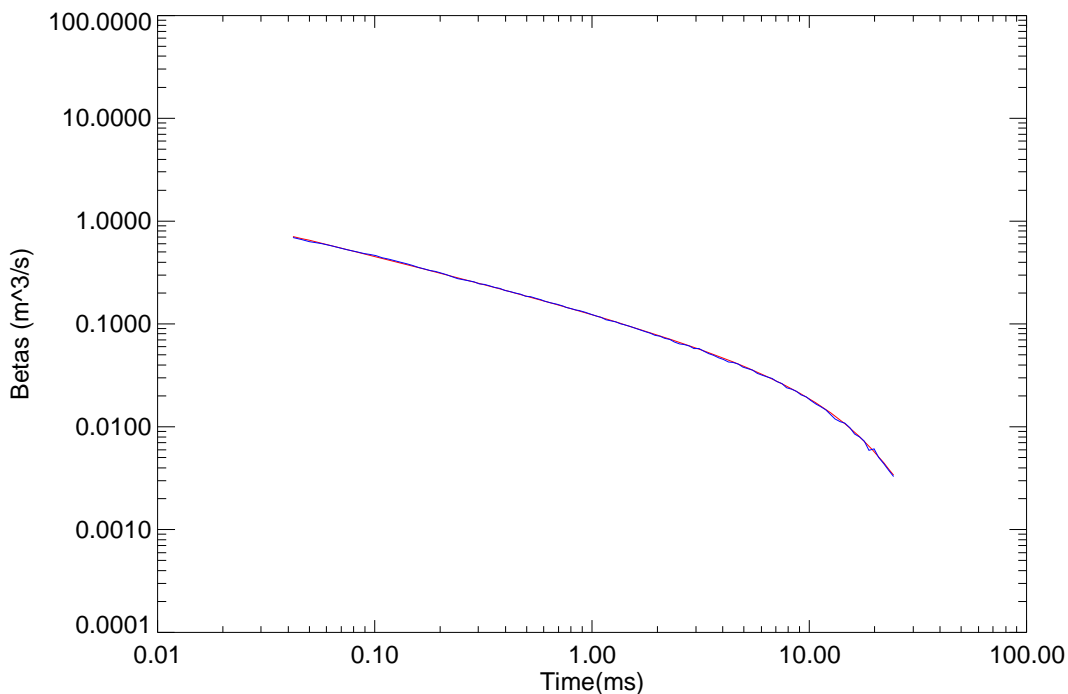


Figure 5-4 – Comparison of measured (blue) versus theoretical (red) polarizability as a function of time for the 4” Aluminum sphere

The Calibration Grid at APG was the first area surveyed and the results were compared with our reference library of parameters prior to completing the data analysis and classification of the results from the Blind Grid and Indirect Fire Areas. Prior to our APG demonstration, we had established a library of target signatures based on test stand measurements. This library was further expanded based on sample targets measured in the pit at APG. Of the 58 ordnance targets present in the Calibration Grid, we were able to correctly identify 53 by matching the inverted signatures to our library. Most of the remaining 5 objects suffered from low signal-to-noise or overlap issues with nearby targets. In Figure 5-5 through Figure 5-7 we show the match between Calibration Grid cells H1, I6, and K3, and our library 60mm and 81mm Mortar and 105mm Projectile, respectively.

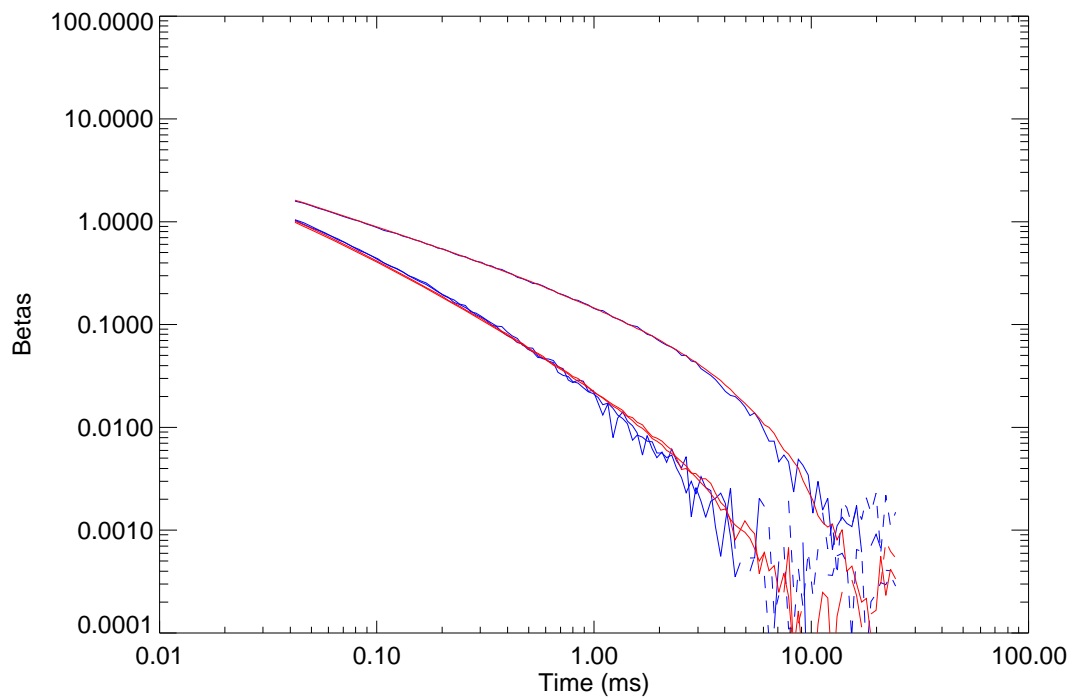


Figure 5-5 – Comparison of measured (blue) versus library (red) polarizability as a function of time for Calibration Area item H1, 60mm Mortar

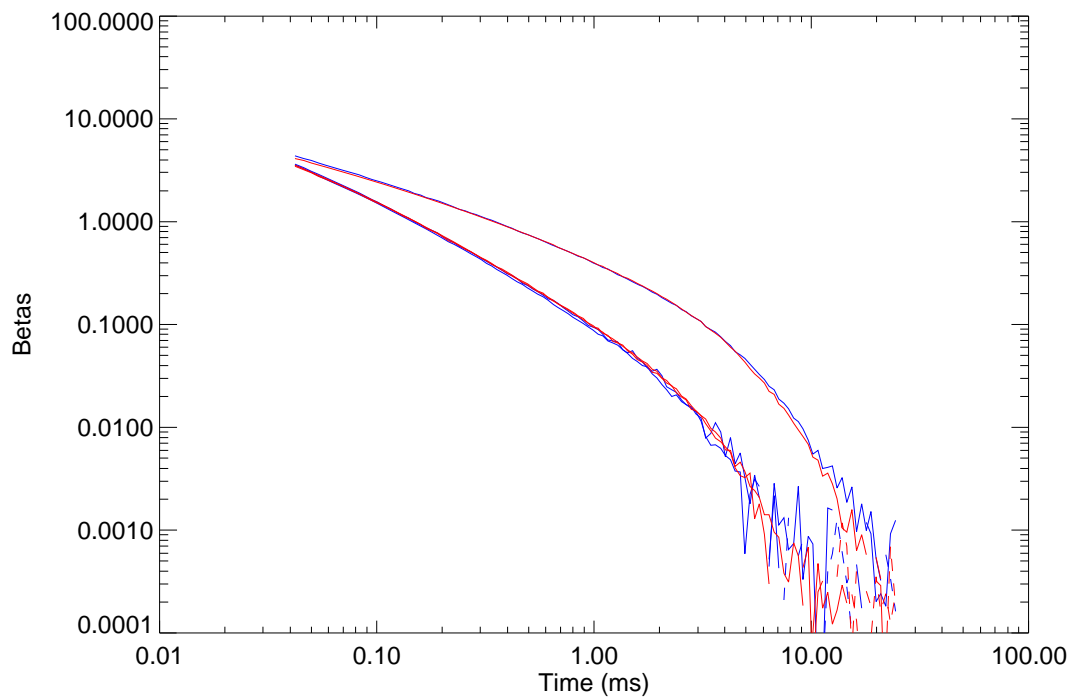


Figure 5-6 – Comparison of measured (blue) versus library (red) polarizability as a function of time for Calibration Area item I6, 81mm Mortar

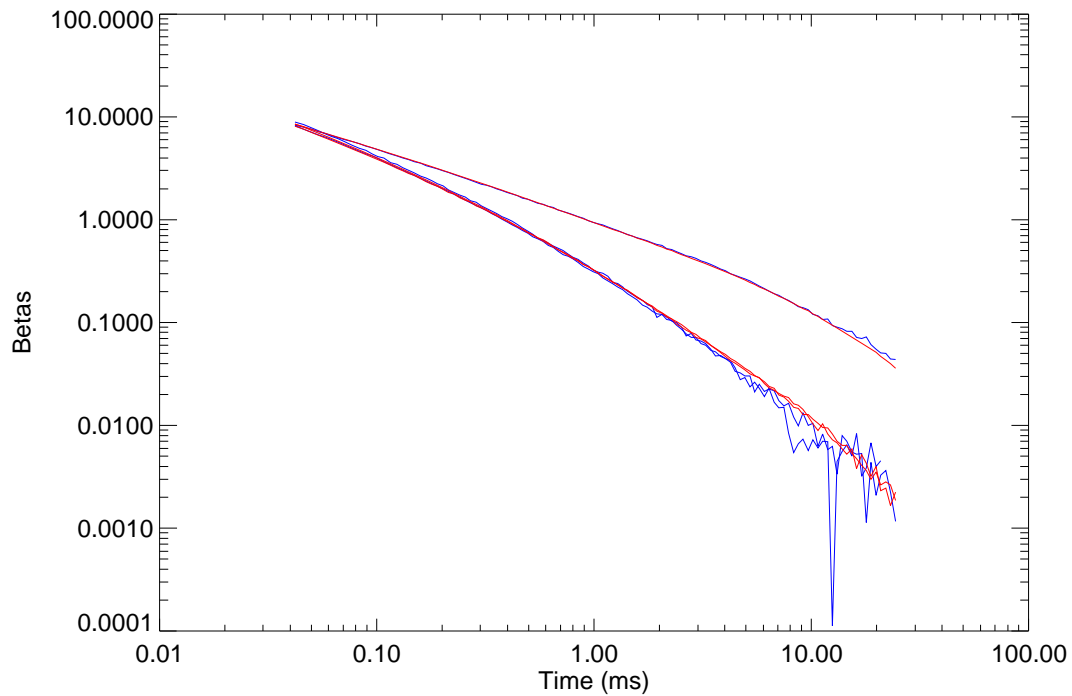


Figure 5-7 – Comparison of measured (blue) versus library (red) polarizability as a function of time for Calibration Area item K3, 105mm Projectile

As this was the first demonstration of the Discrimination Array, the effect of background variation from point to point and over time was not fully understood and remains an object of study. As such, frequent backgrounds were taken over the course of each field day for immediate use for background subtraction and future analysis regarding issues of background variability and the impact on fit parameter extraction. Nine background locations were identified from the magnetometer data as being ‘quiet’ or having a very low background response level. The selected locations were positioned throughout the site to minimize the drive time to a background point from any position on the field. The locations are shown in Figure 5-8 and listed in Table 5-1.

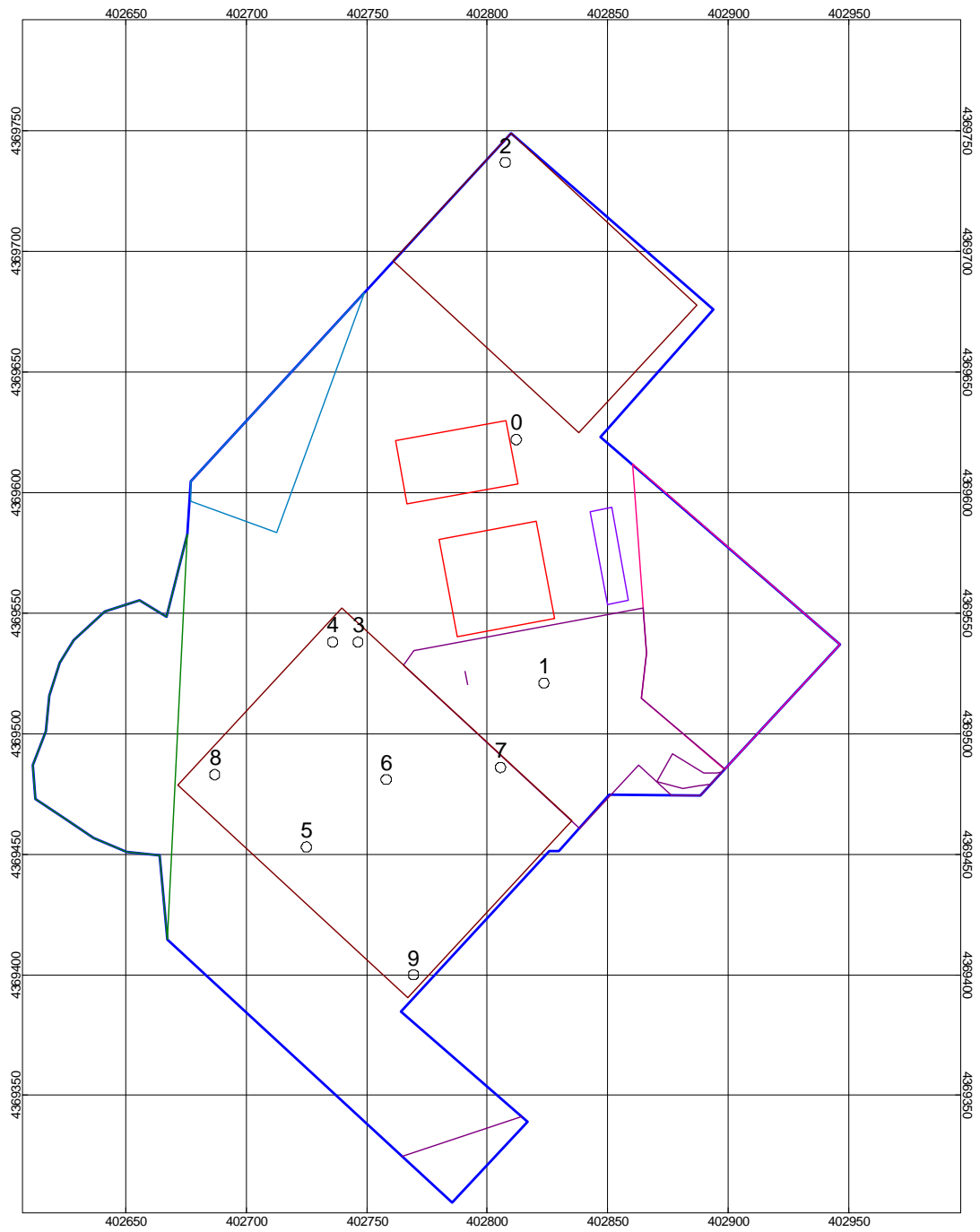


Figure 5-8 – Discrimination Array background measurement locations. The boundaries of the ATC test field areas are shown for reference.

Table 5-1 – Discrimination Array background measurement locations

<b>Fiducial</b>	<b>Easting (m)</b>	<b>Northing (m)</b>	<b>Service Area</b>
0	402,812.00	4,369,622.00	Calibration / Blind Grid
1	402,823.50	4,369,521.00	Challenge
2	402,807.50	4,369,737.00	Direct Fire
3	402,746.40	4,369,538.00	IDF
4	402,735.90	4,369,538.00	IDF
5	402,725.00	4,369,453.00	IDF
6	402,758.10	4,369,481.00	IDF
7	402,805.50	4,369,486.00	IDF
8	402,687.00	4,369,483.00	IDF
9	402,769.40	4,369,400.00	IDF

## **5.5 DATA COLLECTION PROCEDURES**

### **5.5.1 Scale of Demonstration**

The demonstration was conducted at the APG Standardized UXO Test Site. A magnetometer survey was conducted on the Calibration and Blind Grids, as well as the Indirect Fire Area (approximately 4.3 acres) on May 7, 2008. The Discrimination Array surveyed the Calibration and Blind Grids. The array was also deployed to approximately 700 anomalies in the Indirect Fire Area that were detected from the magnetometer data set. The Discrimination Array portion of the demonstration occurred from June 16 – 23, 2008.

### **5.5.2 Sample Density**

Magnetometer data were collected with nominal down-track spacing of 6 cm and cross track spacing of 25 cm. EMI data spacing is fixed at 40 cm in both directions by the array design.

### **5.5.3 Quality Checks**

Preventative maintenance inspections were conducted continually by all team members during data collection, focusing particularly on the tow vehicle and sensor trailer. Deficiencies were addressed according to the severity of the deficiency. Parts, tools, and materials for many maintenance scenarios are available in the system spares inventory, a fraction of which was on site. The remainder was available at our base of operations at Blossom Point, MD.

For the magnetometer array, the following data quality checks and procedures were used to insure a quality data product. MTADS magnetometer survey raw data generally falls into two categories, location and magnetometer sensor measurements. The data set is comprised of ten separate files, each containing the data from a single system device. Each device has a unique data rate. A software package written by NRL examines each file and compares the number of entries to the product (total survey time \* data rate). Any discrepancies are flagged for the data analyst to address.

For magnetometer sensor data, operational values are typically on the order of 50,000 nT and have noise levels of ~0.5 nT peak-to-peak (PP) static and 3-5 nT PP in motion. Sensor “drop-outs” can occur if the sensor is tilted out of the operation zone with respect to the earth’s magnetic field. If a sensor cable is severed or damaged while in motion, the sensor output value will drop below 20,000 nT and/or become very noisy (1,000’s of nT PP). All magnetometer sensor channels (8 total) were examined in each survey file set for these conditions and any data which are deemed unsatisfactory was flagged and not processed further.

For location data, the RTK GPS receivers present a Fix Quality value that relates to the quality / precision of the reported position. A Fix Quality (FQ) value of 3 (RTK Fixed) is the best accuracy (typically 3-5 cm or better). A FQ value of 2 (RTK Float) indicates that the highest level of RTK has not been reached yet and location accuracy can be degraded to as poor as ~1 m. FQs 1 & 4 correspond to the Autonomous and DGPS operational modes, respectively. Data collected under FQ 3 and FQ 2 (at the discretion of the data analyst) were retained. Any other data were deemed unsatisfactory, flagged, and not processed further. The section of data containing the flagged data was logged for future re-acquisition as required. Additionally, any identified gaps in data coverage were brought to the survey team’s attention for further data collection. Data which meet these standards are of the quality typical of the MTADS system.

Since the Discrimination Array operates in a cued mode, the data QC procedures and checks differ from the survey mode instruments. The status of the RTK GPS system can be visually determined by the operator prior to starting the data collection cycle, assuring that the position and orientation information are valid (FQ 3) during the collection period.

Two data quality checks were performed on the TEM array data. After background subtraction, contour plots of the signal were generated for the 25 transmit/receive pairs at a decay time of 0.042 ms. An example of a good data set from a single anomaly with a large SNR is shown in Figure 5-9 for Calibration Area item I6. The plots were visually inspected to verify that there was a well defined anomaly without extraneous signals or dropouts. QC on the transmit/receive cross terms was based on the dipole inversion results. Our experience has shown that data glitches show up as reduced dipole fit coherence. No data glitches were observed during our APG demonstration, so data collected at our Blossom Point facility for a 105mm HEAT Projectile are used as an example. The fit polarizabilities as a function of decay time are shown with all elements (Figure 5-10) and with element 21 excluded (Figure 5-11), with fit coherences of 0.699 and 0.992 respectively. In comparing Figure 5-10 and Figure 5-11, the expected axial symmetry of the minor polarizabilities is restored with the exclusion of element 21 in this case. The problem with element 21 is only observable at late time and therefore would not be captured in the monostatic plot review.

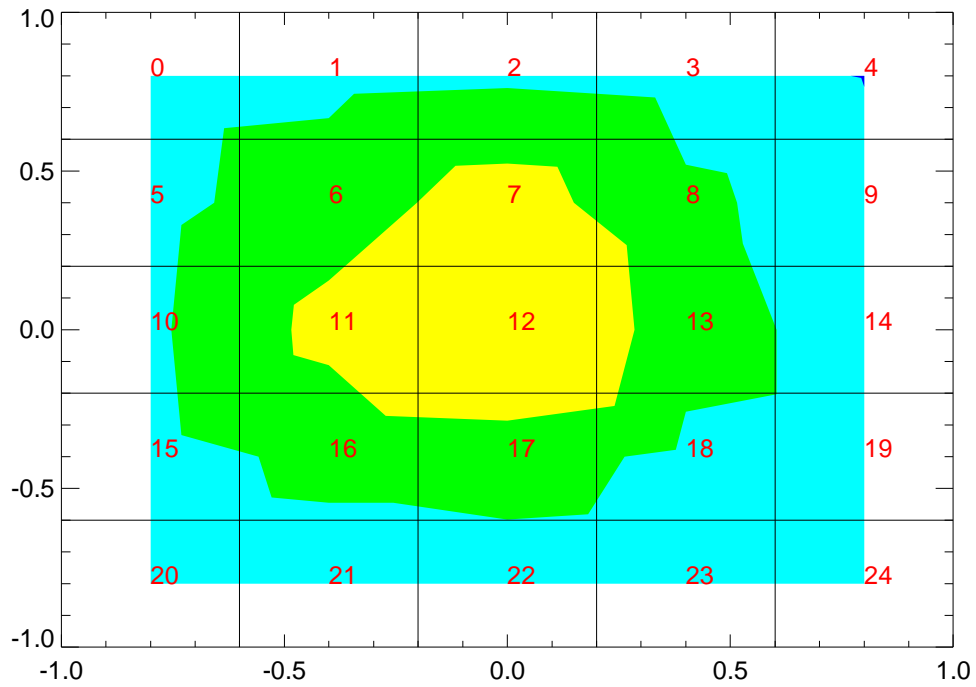


Figure 5-9 – Monostatic QC contour plot for Calibration Area item I6

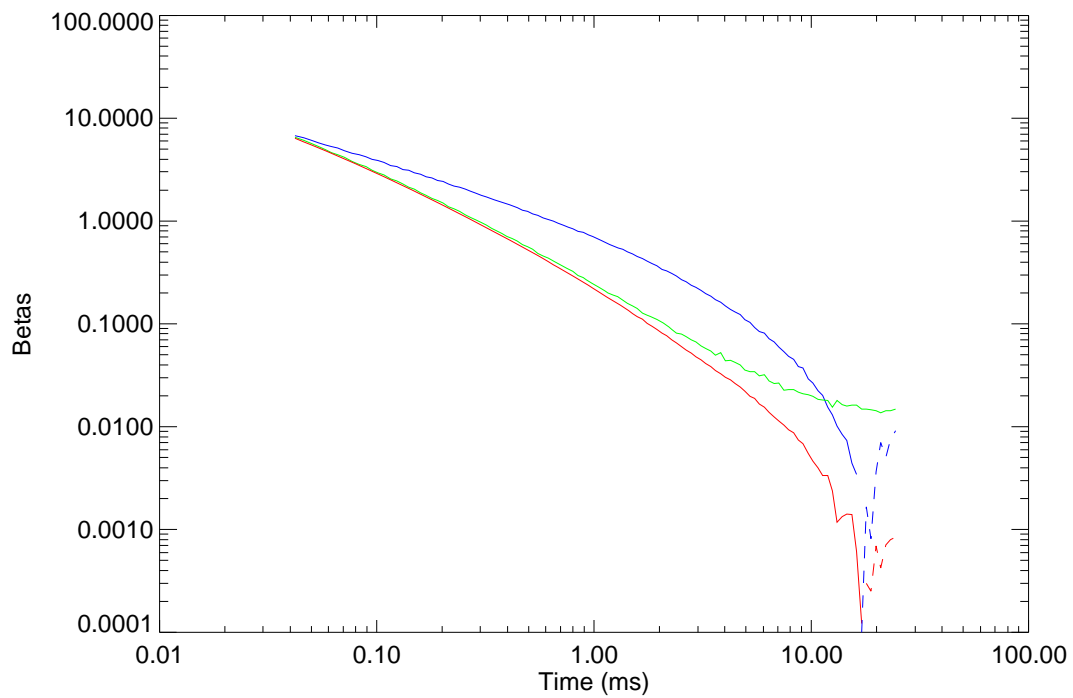


Figure 5-10 – Polarizability as a function of time for a 105mm HEAT Projectile with all data included. The fit coherence for all elements included was 0.699.



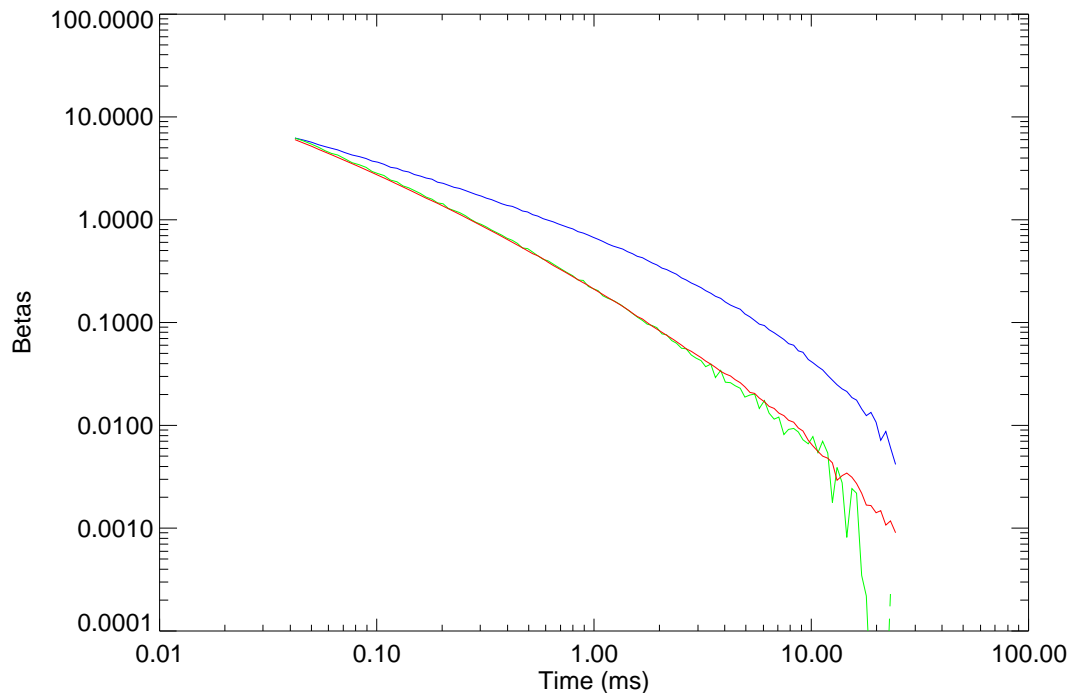


Figure 5-11 – Polarizability as a function of time for a 105mm HEAT Projectile with element 21 excluded. The fit coherence with element 21 excluded was 0.992.

The issue of when multiple objects are found to be under the array simultaneously, generating overlapping signatures, can also be addressed at this point in the data QC process. An example case is shown in Figure 5-12. There are two apparent issues in the data set. First, there appears to be a small, shallow bit of scrap on top of the target. Second, there was a bit of scrap present in the background file used. This latter issue is seen in the data from element 0. Figure 5-13 shows the fit betas obtained using all of the data. Figure 5-14 shows the fit betas obtained excluding elements 0,5,10,11,15,16,17,20,21,22. The latter betas match our library 105mm HEAT betas very well.

Any data set that was deemed unsatisfactory by the data analyst, was flagged and not processed further. The anomaly corresponding to the flagged data was logged for future re-acquisition. Data which meet these standards are of the quality typical of the MTADS system.

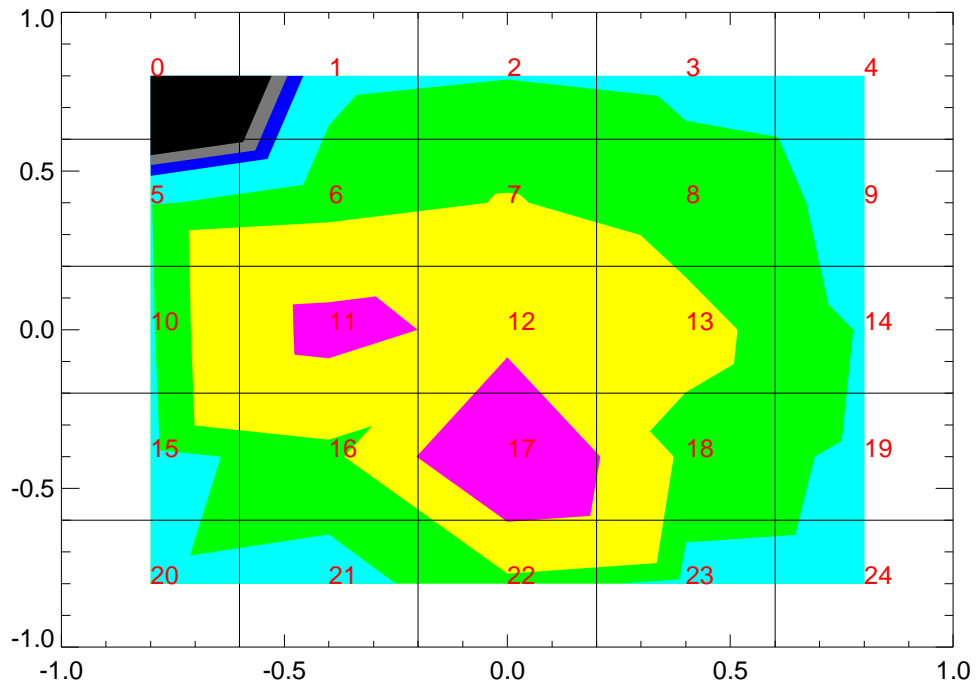


Figure 5-12 – Monostatic QC contour plot for example anomaly

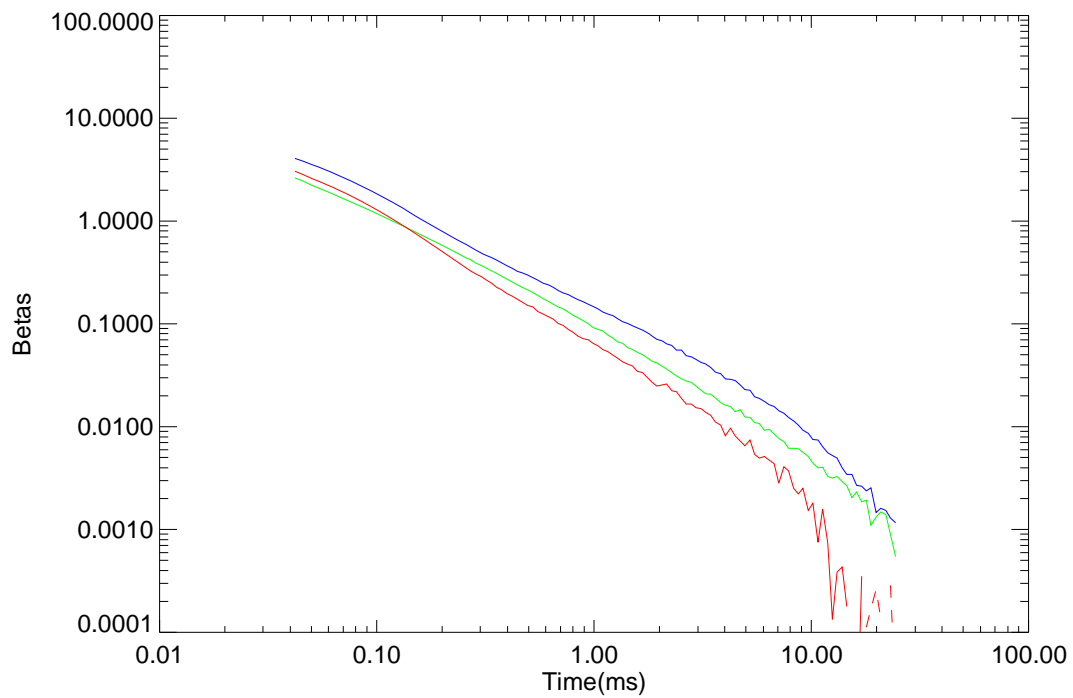


Figure 5-13 - Polarizability as a function of time for the example show in Figure 5-12 with all data included. The fit coherence for all elements included was 0.652.

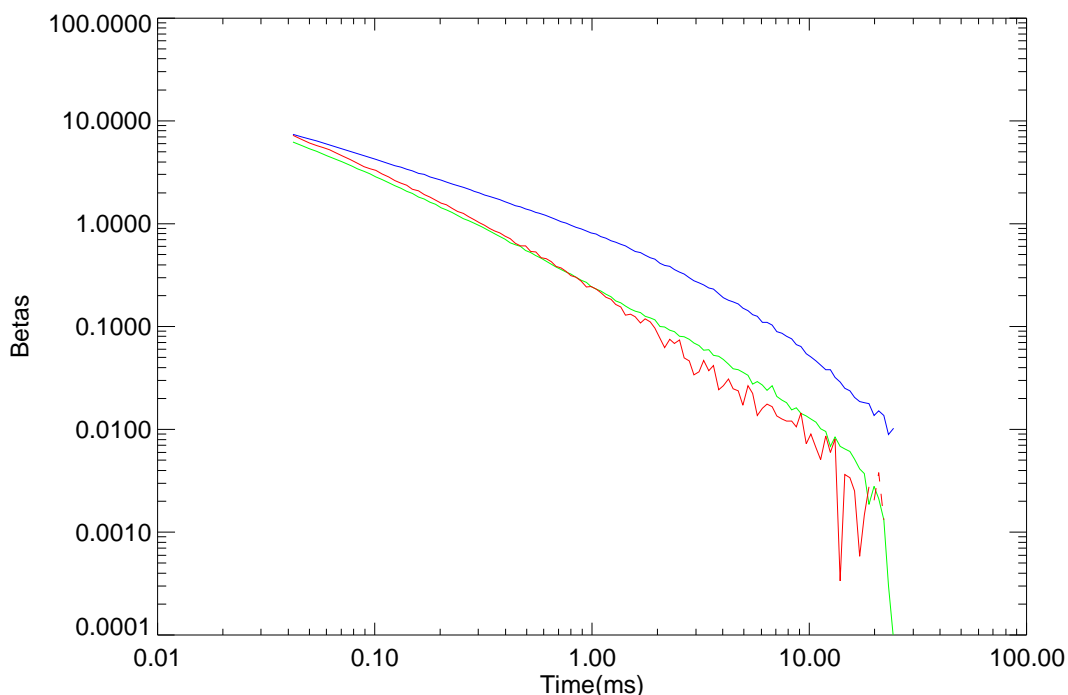


Figure 5-14 - Polarizability as a function of time for the example show in Figure 5-12 with elements 0,5,10,11,15,16,17,20,21,22 excluded. The fit coherence for the remaining elements was 0.985.

#### 5.5.4 Data Handling

Data were stored electronically as collected on the MTADS vehicle data acquisition computer hard drives. Approximately every two survey hours, the collected data were copied onto removable media and transferred to the data analyst for QC/analysis. The data were moved onto the data analyst's computer and the media recycled. Raw data and analysis results were backed up from the data analyst's computer to optical media (CD-R or DVD-R) or external hard disks daily. These results are archived on internal file servers at NRL or SAIC. Refer to Reference 7 for specific details on the magnetometer system file formats. Examples of the Discrimination Array file formats are provided in Appendix B. All field notes / activity logs were written in ink and stored in archival laboratory notebooks. These notebooks are archived at NRL or SAIC. Relevant sections are reproduced in demonstration reports such as this. Dr. Tom Bell is the POC for obtaining data and other information. His contact information is provided in Appendix A of this report.

#### 5.5.5 Magnetometer Survey Data Summary

The MTADS tow vehicle and magnetometer array were mobilized to the APG Test Site on May 6, 2008. The magnetometer portion of the demonstration was conducted the following day, May 7, 2008. A standard MTADS magnetometer survey of the Calibration, Blind Grid, and the Indirect Fire Area of the Standardized Site was conducted. Anomaly locations were manually

identified from the data for the Blind Grid and in a combination threshold exceedance / manual review method for the Indirect Fire Area as described in Section 6.2 below. A data segment around each anomaly center was extracted and analyzed using the UX-Analyze subsystem of the Oasis montaj software package as described in Section 6.2 to fit the data to a dipole model and extract the associated fit parameters (position, depth, equivalent size). These fit results constituted the source anomaly lists for the Blind Grid and Indirect Fire Areas for the Discrimination Array stage of the demonstration.

In practice, the majority of the site was surveyed as a whole with the magnetometer system and the resulting data were analyzed in parallel to the above effort. The results were provided to the Program Office in support of the recent reconfiguration effort. Anomalies were detected in a manner similar to that used for MTADS data sets collected as part of the ESTCP UXO Discrimination Study at the former Camp Sibert [7].

#### **5.5.6 Calibration Area**

The ground truth for the Calibration Area is known and the collected data were used to verify the operational status of our systems and processing procedures. A magnetometer anomaly map of the data is shown in Figure 5-15. The reported location and identification of the seeded items are also indicated in the figure. An amplitude scale of  $\pm 10$  nT was used for comparison as the threshold exceedance amplitude for the Indirect Fire Area was set at 4 nT.



not added to the Discrimination Array anomaly list. An Excel spreadsheet detailing all Blind Grid anomalies is included on the accompanying DVD (APG\_BlindGrid\_PickedCells.xls).

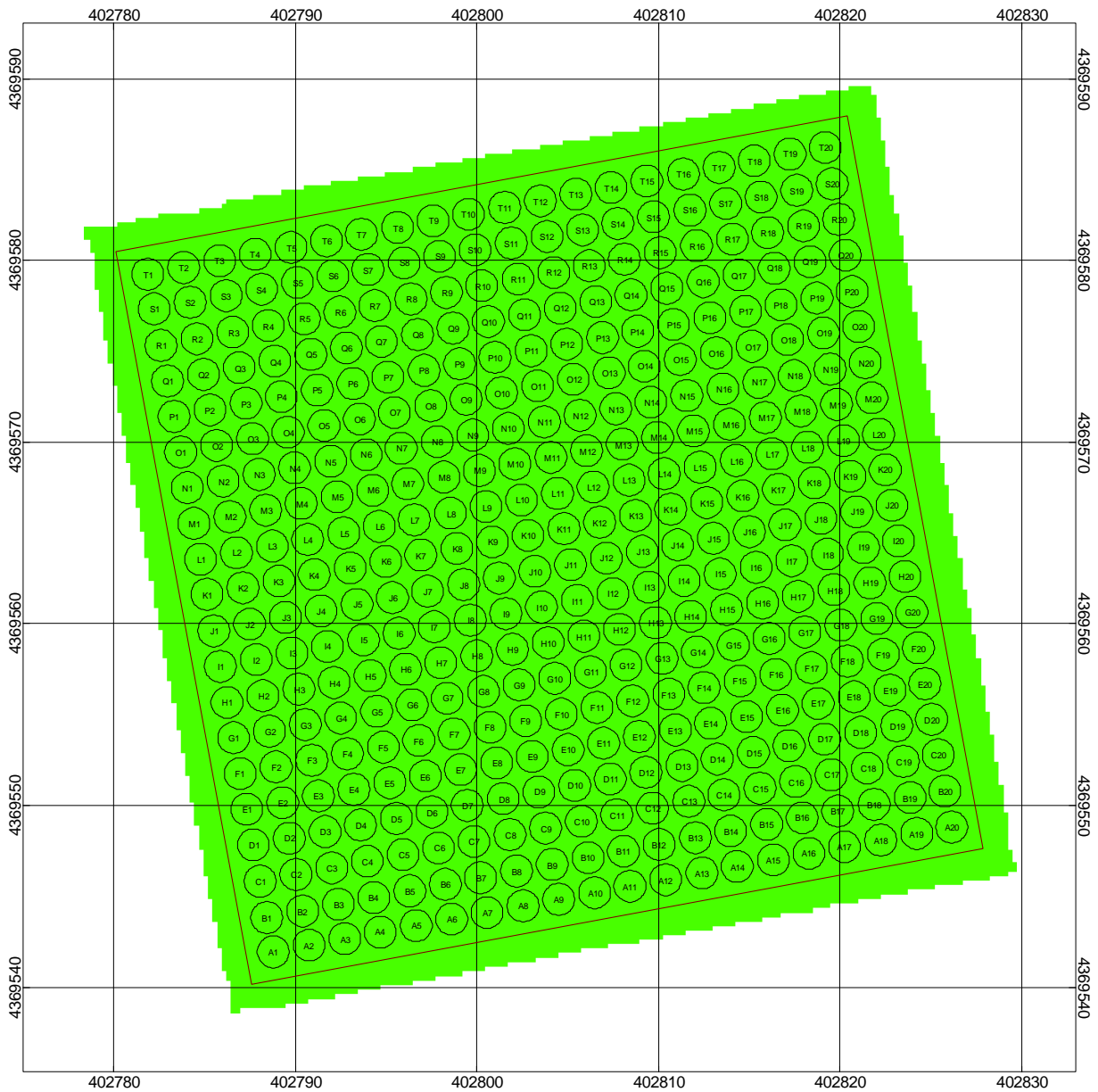


Figure 5-16 – Magnetometer system coverage map for the APG Blind Grid.

### 5.5.8 Indirect Fire Area Response Curves

The Indirect Fire Area (IDF) is seeded with three munitions types, the 60mm and 81mm Mortar and the 105mm Projectile. Prior to deployment to APG, a series of test-pit measurements were made at Blossom Point in a similar manner to those made for the ESTCP UXO Discrimination Study at the former Camp Sibert [7]. Example items of each of the three munitions type were acquired from ATC as part of a standard munitions set for the measurements. Figure 5-17 through Figure 5-19 show both the measured peak positive response for each item and the dipole model bounding curves for each item. The RMS background signal level for several ‘quiet’ patches of magnetometer data were determined and averaged to get a measure of the overall site background level. The average value was found to be 1.5 nT ( $1\sigma$ ). Based on the system response to the three munitions, the minimum threshold exceedance value was found to be 5.3 nT for the 60mm Mortar at a depth of 11x. With the 25% safety margin applied, a final threshold of 4 nT was set.

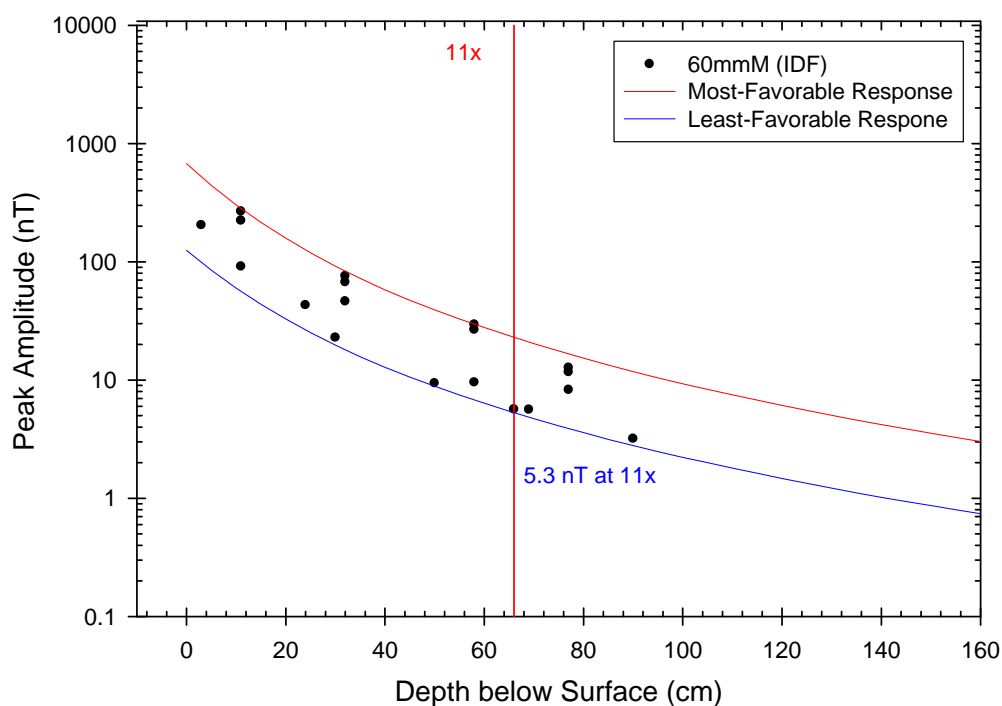


Figure 5-17 – Magnetometer response curve for the ATC standard 60mm Mortar

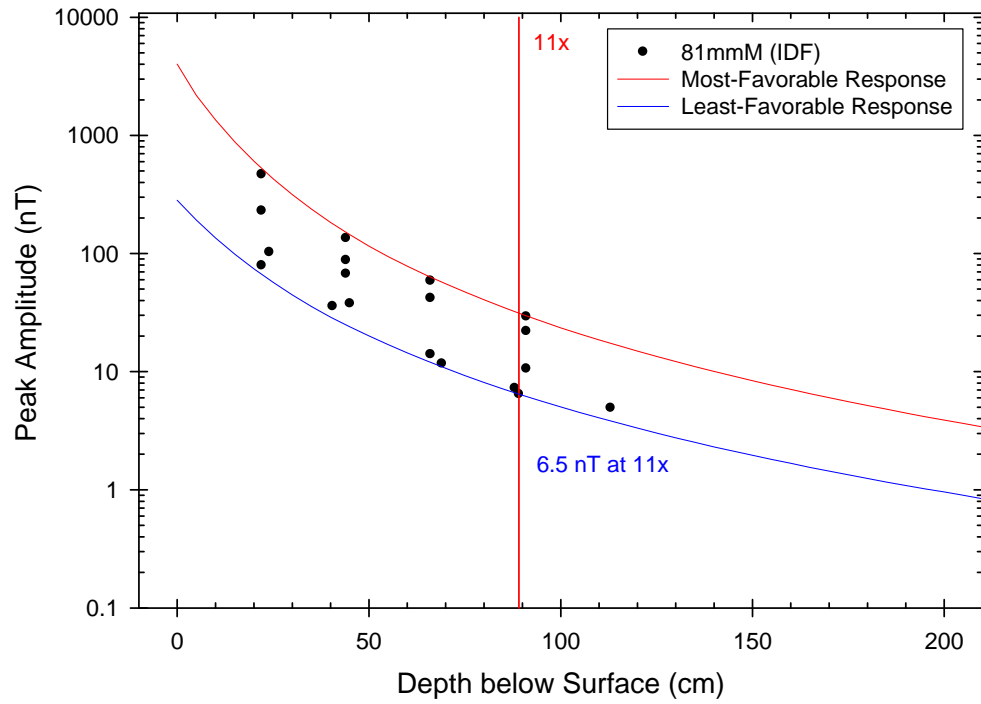


Figure 5-18 – Magnetometer response curve for the ATC standard 81mm Mortar

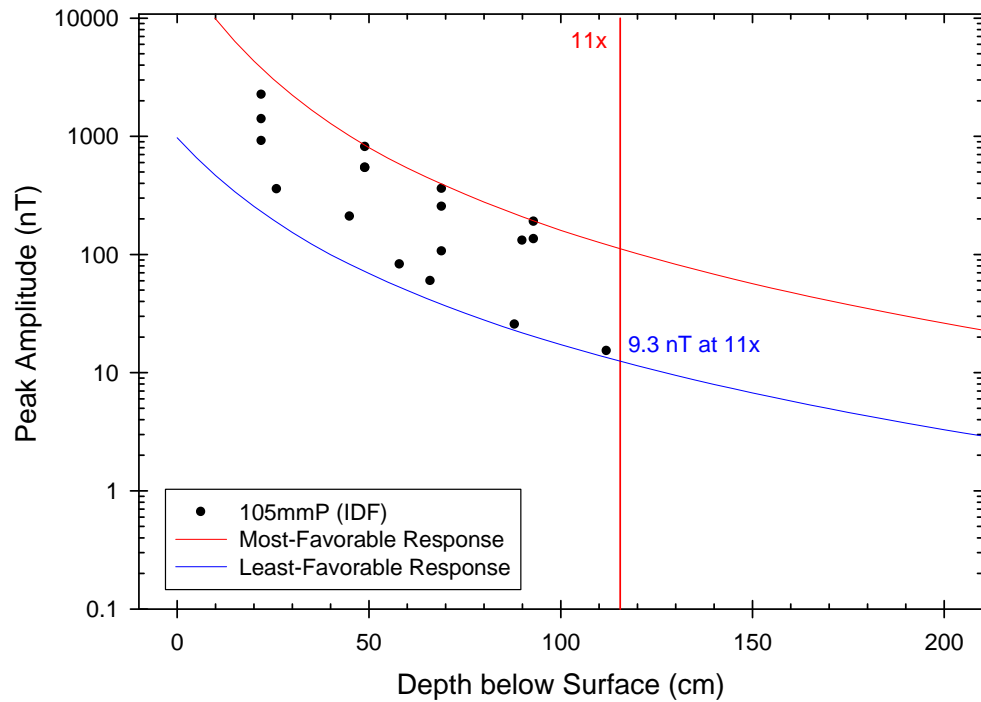


Figure 5-19 – Magnetometer response curve for the ATC standard 105mm Projectile



### 5.5.9 Indirect Fire Area

The Indirect Fire Area is a 1.3 ha area drawn from the original configuration's Open Field. The IDF has been seeded with three munitions types, the 60mm and 81mm Mortar and the 105mm Projectile. Based on the response curve results presented in Section 5.5.8, an anomaly detection threshold of 4 nT was selected and used for an initial anomaly detection screen of the IDF magnetometer data. Only the positive lobe of the dipolar response is detected in this fashion. 1,301 anomalies were detected in the data set. A data segment around each anomaly center was extracted and analyzed using the UX-Analyze subsystem of the Oasis montaj software package as described in Section 6.2 to fit the data to a dipole model and extract the associated fit parameters (position, depth, equivalent size). These results were then given to an experienced data analyst to review each anomaly individually, manually adjust the data segment boundary as necessary, and review the data set as a whole for any anomalies missed by the automated routine. Fit parameters for the final list of 1,310 anomalies were determined and are provided as an Excel spreadsheet on the accompanying DVD (APG\_IDF\_FitResults.xls). The data analyst classified each anomaly into one of the ten categories listed in Table 5-2. The 694 anomalies in Ranks 1, 2, 3, and 7 were added to the IDF anomaly list for the Discrimination Array. The anomalies in the other categories could reasonably be excluded as not potentially arising from one of the three seeded munitions.

Table 5-2 – Ranking categories for IDF magnetometer anomalies and number of anomalies in each category

Rank	Number of Anomalies	Description
1	423	Decent fit with a size between a 60mm and 105mm
2	65	Poor fits (<.8 fit coherence) but would recommend taking cued data because of the shape/size of the anomaly
3	132	Would not fit but would recommend taking cued data because of the shape/size of the anomaly
4	334	Fits but size too small for a 60mm (A rough cutoff of 0.030m in the Fit_Size channel was used)
5	79	Anomaly caused by array bounce noise/geology
6	12	Anomaly caused by data processing artifacts
7	74	Fits but show high remnant magnetization (A conservative cutoff of 80 degrees in the Fit_SolidAngle was used)
8	101	Poor fit (<.8 fit coherence) likely small clutter or noise
9	85	Would not fit – likely small clutter or noise
10	5	Fits but size larger than a 105mm (A cutoff of 0.175m in the Fit_Size channel was used)

A magnetometer system coverage map is shown in Figure 5-20. The two white areas shown in Figure 5-20 represent two portions of the Indirect Fire Area that were not accessible to the magnetometer system during the first portion of the demonstration.

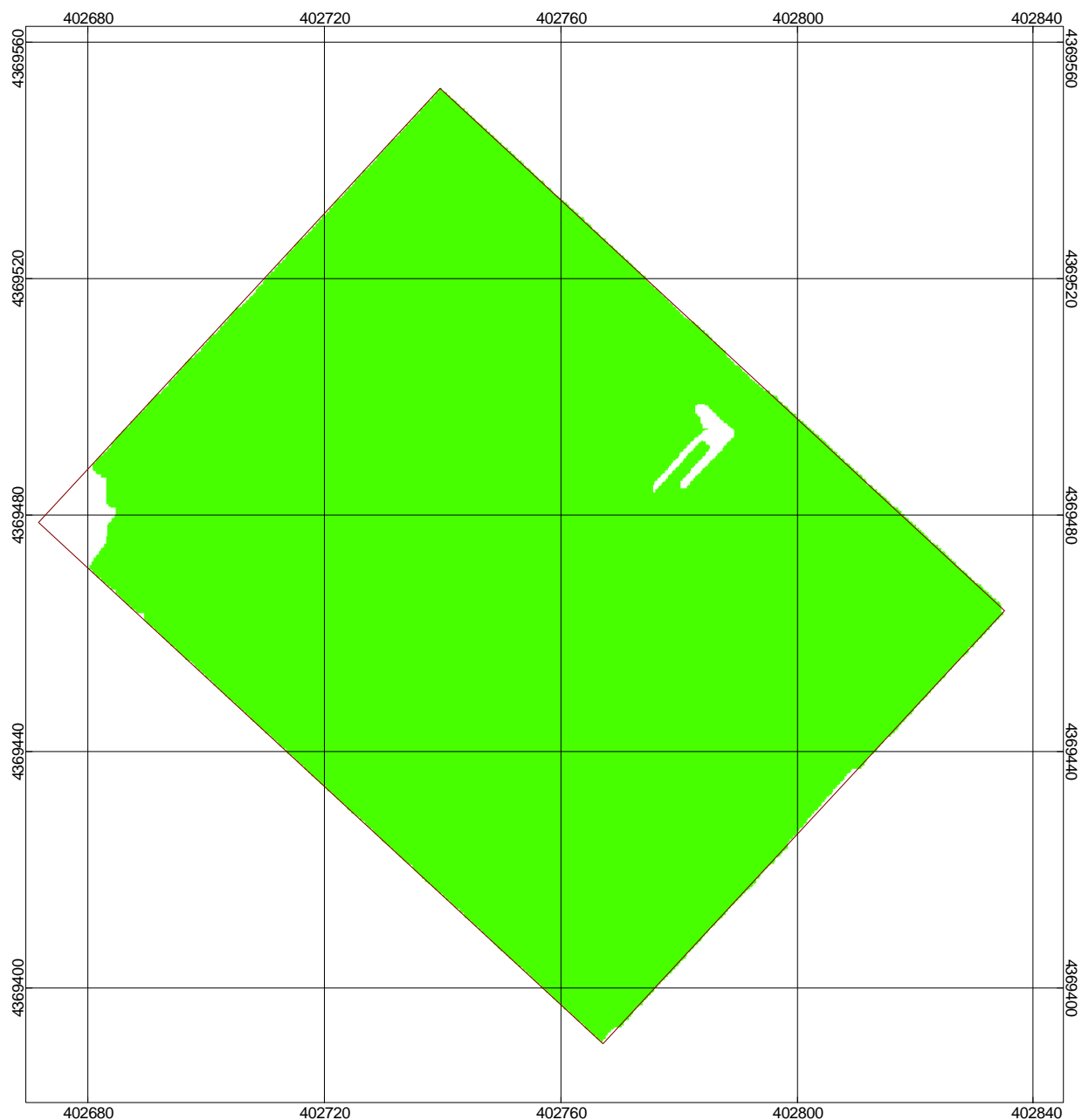


Figure 5-20 – Magnetometer system coverage map for the APG Indirect Fire Area.

#### 5.5.10 Discrimination Survey Data Summary

The MTADS tow vehicle and Discrimination Array were mobilized to the APG Test Site during the week of June 9, 2008. A shipping container was delivered on May 30, 2008 to augment the onsite secure storage facilities. The Discrimination Array portion of the demonstration commenced on June 16, 2008 with a data collection in the Calibration Area. Cued surveys were

conducted of the Calibration, Blind Grid, and the Indirect Fire Area. Data collection was completed on June 23, 2008. The system was demobilized later that week to our Blossom Point facilities. The shipping container was removed on June 27, 2008.

The array was positioned roughly over the center of each anomaly on the source anomaly list for each area and a data set collected. Each data set was then inverted using the data analysis methodology discussed in Section 6.0, estimated target parameters determined, and ultimately a classification made for each item for the Blind Grid and Indirect Fire Area.

#### **5.5.11 Calibration Area**

The ground truth for the Calibration Area is known and the collected data were used to verify the operational status of our systems and processing procedures. Each of the 66 seed locations in the Calibration Area was investigated in turn and the resultant fit parameters used to cross-check against and augment our library of responses to known munitions items. Data collection occurred on June 16, 2008. The background-corrected data set for each anomaly is included on the accompanying DVD.

#### **5.5.12 Blind Grid**

The Blind Grid is composed of 400 cells in a 20x20 array with 2m on-center spacing. The Rank 1 and 2 anomalies (214 anomalies) identified in the magnetometer survey (See Section 5.5.7) formed the Blind Grid anomaly list for the Discrimination Array. ATC staff placed a plastic pin flag on the center of each of the 214 anomalies investigated prior to this portion of the demonstration. Data collection occurred during the period June 16 - 17, 2008. The background-corrected data set for each anomaly is included on the accompanying DVD.

#### **5.5.13 Indirect Fire Area**

The Indirect Fire Area is a 1.3 ha area drawn from the original configuration's Open Field. The IDF has been seeded with three munitions types, the 60mm and 81mm Mortar and the 105mm Projectile. The 694 anomalies in Ranks 1, 2, 3, and 7 (See Section 5.5.9) were added to the IDF anomaly list for the Discrimination Array. Data collection occurred during the period June 17 - 23, 2008. The background-corrected data set for each anomaly is included on the accompanying DVD.

#### **5.5.14 Indirect Fire Area Survey Patterns**

The navigation software for the Discrimination Array provides the capacity to guide the operator with cm-level accuracy to place the array over the center of any anomaly on the anomaly list. Determining the most efficient method with which to order the anomalies for data collection was an additional part of this demonstration. The IDF was broken up into 130m long and 20m wide blocks and different ordering techniques were tested and evaluated. The three techniques evaluated were:

- a) Placing a plastic pin flag on each anomaly location and allowing the operator and spotter personal to pick the optimum path on-the-fly. The flag was removed from each anomaly after data collection.

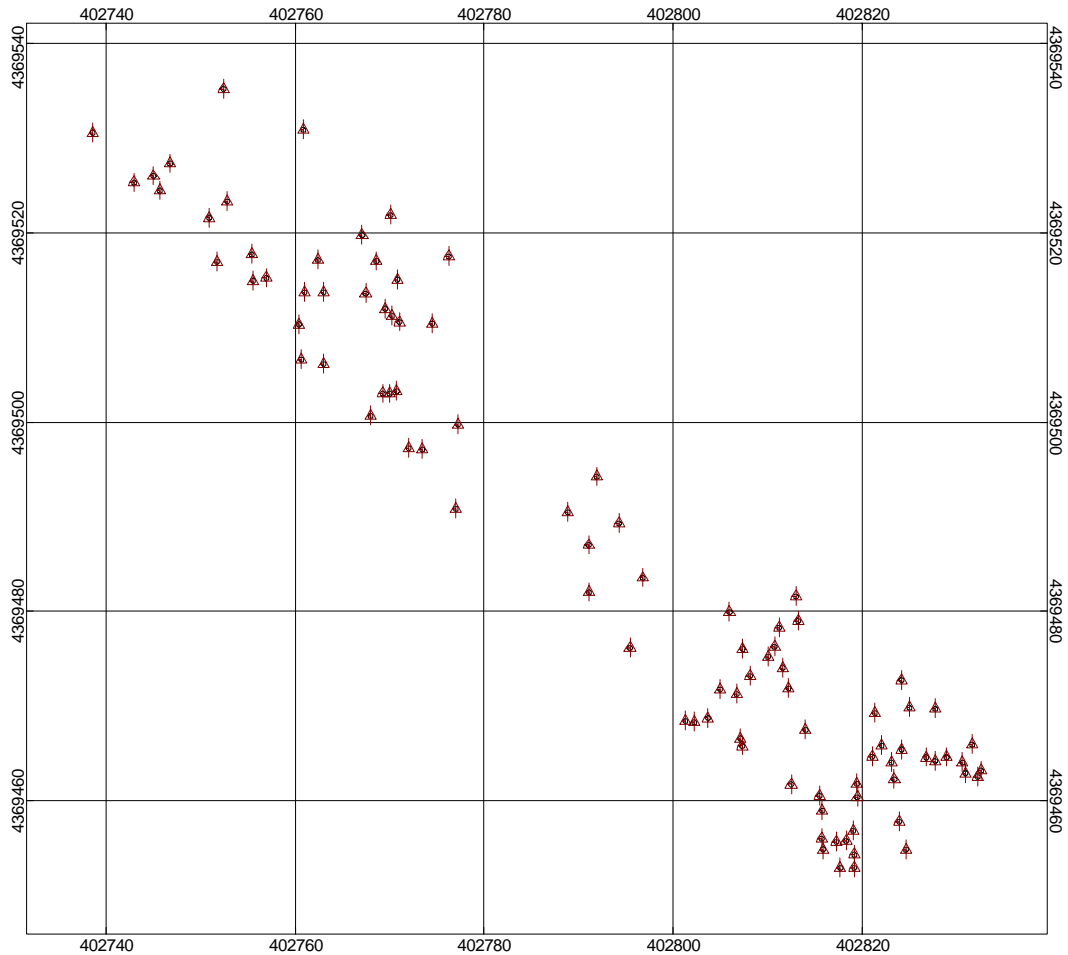


Figure 5-21 – A portion of the Indirect Fire Area with anomaly locations flagged.

- b) Reordering the anomaly list into a pre-planned, alternating direction path where the anomalies were binned into 2m-wide swaths. Each anomaly was investigated in order with a single spotter recording completion of data collection.

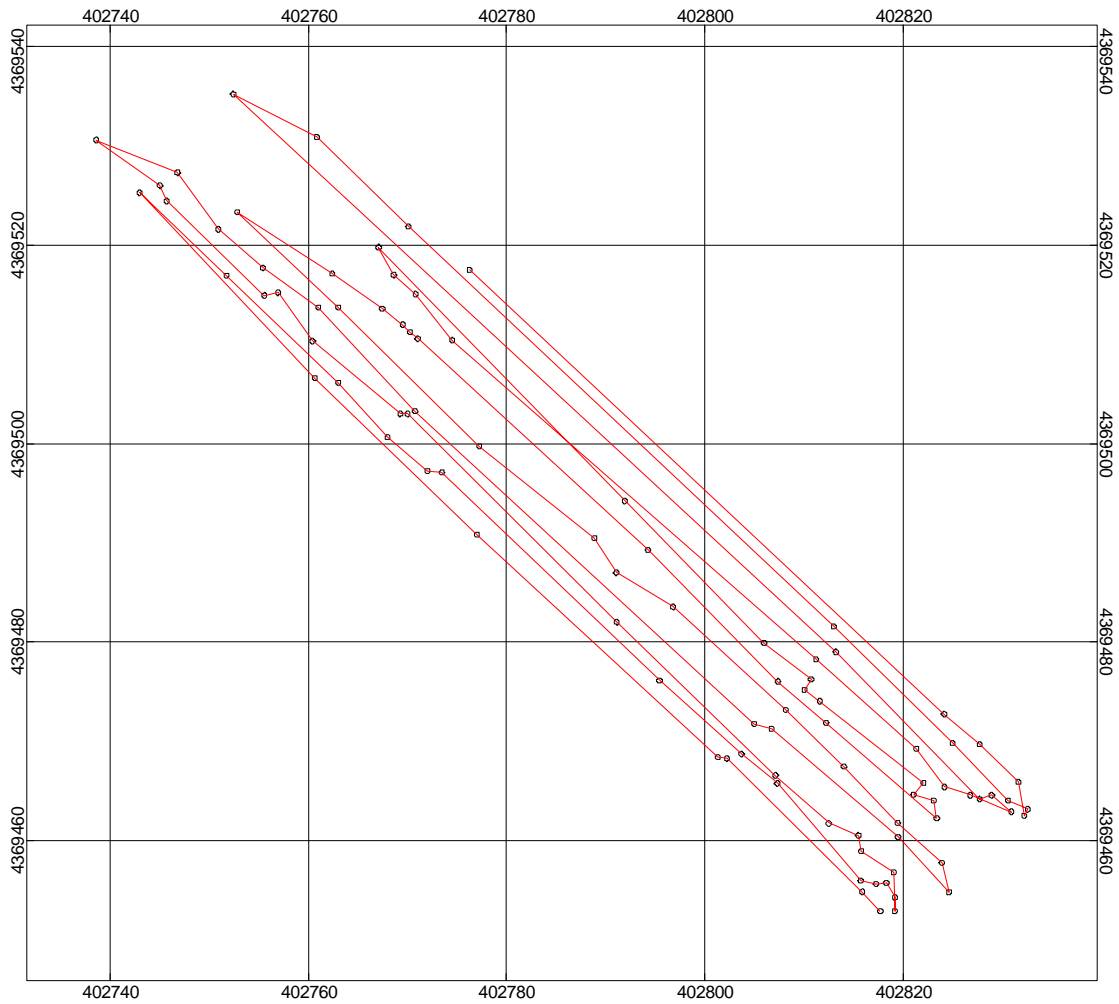


Figure 5-22 – A portion of the Indirect Fire Area with anomalies binned into 2-m swaths. The anomalies are shown in black, the planned route is shown in red.

- c) Reordering the anomaly list into a pre-planned, alternating direction path where the anomalies were binned into 1m-wide swaths. Each anomaly was investigated in order with a single spotter recording completion of data collection.

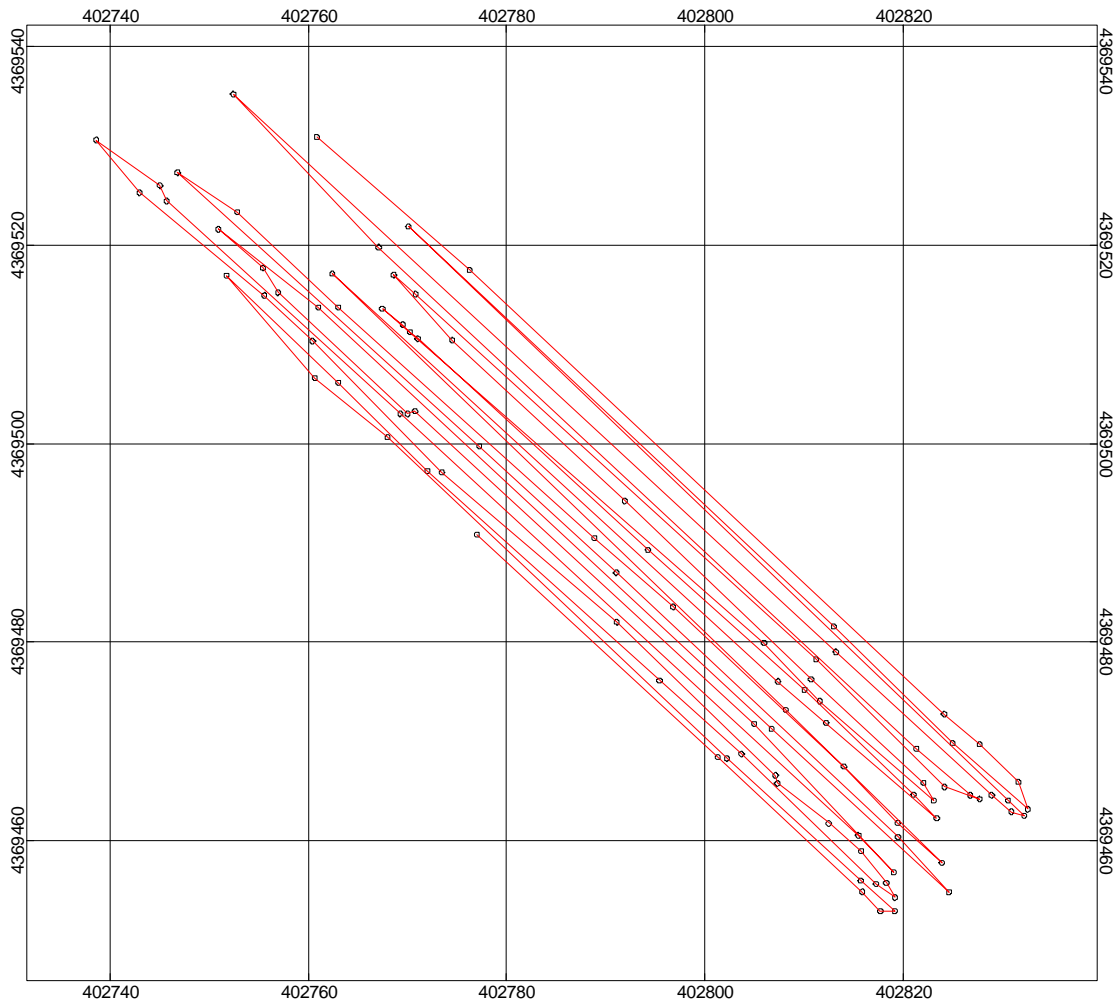


Figure 5-23 – A portion of the Indirect Fire Area with anomalies binned into 1-m swaths. The anomalies are shown in black, the planned route is shown in red.

Each of the three techniques was evaluated for an entire 20-m segment of the field. All three techniques were found to be equally effective for our practiced survey team, especially for the vehicle operator. Production rates of greater than 200 anomalies / day were maintained for the entire demonstration. Based on discussions with the operator, the 2-m swath technique requires significant skill in precisely placing the sensor array on the anomaly including while backing up. The narrower potential solid angle for the 1-m swaths is expected to make it easier for less-skilled operators to maintain peak efficiency. The pin flag technique is also very efficient but requires a significant amount of setup and takedown for the flag placement.

## **5.6 VALIDATION**

With the exception of the Calibration Grid, the ground truth for the Standardized sites is held back from individual technology demonstrators to preserve the utility of the Blind Grid and Open Field Areas. Results from the Blind Grid and the Indirect Fire Area were submitted to ATC for performance evaluation. Scoring results have been received and are available [12]. A summary of the results are given in Section 7.0.

## **6.0 DATA ANALYSIS PLAN**

The MTADS Discrimination Array is a cued UXO classification system. There were two parts to the data collection in this demonstration: an initial magnetometer survey which served primarily to locate targets, and TEM array measurements over the targets detected in the magnetometer survey. The TEM data were used for target classification and discrimination. Target depths determined from the initial magnetometer survey data were reviewed but not used cooperatively with the TEM array data in the target classification and discrimination analysis as discussed in Section 6.3.

### **6.1 PREPROCESSING**

The collected raw magnetometer data were preprocessed on site for quality assurance purposes using standard MTADS procedures and checks. The various data files were merged and imported into a single Oasis montaj (v6.4, Geosoft, Inc.) database using custom scripts developed from the original MTADS DAS routines which have been extensively validated.

As part of the import process any data corresponding to a magnetometer outage, a GPS outage, or a vehicle stop / reverse, were defaulted or marked to not be further processed. Defaulted data were not deleted and can be recovered at a later time if so desired. Any long wavelength features such as the diurnal variation of the earth's magnetic field and large scale geology were filtered from the data (demedianed).

The located, demedianed magnetometer data were then imported into UX-Analyze for individual anomaly analysis. The data surrounding the center of each selected anomaly were extracted and submitted to the physics-based models resident in UX-Analyze to determine anomaly size, position, and depth. A spreadsheet containing details of the anomaly location and fit parameters is provided on the accompanying DVD. The located demedianed magnetometer data were exported into an ASCII format for delivery and for archival purposes and are provided on the accompanying DVD.

The TEM array has 25 transmitters/receiver pairs. For each transmit pulse, the response measured at all of the receivers was recorded simultaneously. For each target, a  $25 \times 25 \times N$  data array is generated, where  $N$  is the number of recorded time gates. The current system configuration bins the data in 121 logarithmically spaced gates. During the preprocessing step, the recorded signals are normalized by the transmitter currents to account for any transmitter variations. To account for time delay due to effects of the receive coil and electronics, we

subtract 0.028 ms from the nominal gate times [13]. The delay was previously determined empirically by comparing measured responses for test spheres with theory. The measured responses include distortions due to transmitter ringing and related artifacts out to about 40  $\mu$ s. Consequently we only included the responses from decay times beyond 40  $\mu$ s in our analyses. This leaves 115 gates spaced logarithmically between 0.040 ms and 25 ms.

The background response was subtracted from each target measurement using data collected in a nearby target-free region, or background. Background locations were selected from quiet areas observed in the magnetometer anomaly map. All of the background measurements were inter-compared to evaluate background variability and to identify outlier measurements potentially corresponded to measurements over non-ferrous targets. We have not observed significant background variability in our measurements at our Blossom Point test site, and were able to use blank ground measurements from 100 meters away for background subtraction on targets in the test field.

Geo-referencing of the array data is based on the GPS data, which gives the location of the center of the array and the orientation of the array. Sensor locations within the array are fixed by the array geometry. Dipole inversion of the array data (Section 6.3) determines target location in local array-based coordinates. The local position was then transformed to absolute coordinates using the array location and orientation determined from the corresponding GPS data.

## **6.2 TARGET SELECTION FOR DETECTION**

Targets were selected from the magnetometer survey data using the threshold exceedance method described in Reference 7 using a physics-based threshold in Oasis montaj for the Indirect Fire Area. An occupied or not occupied decision was had for each Blind Grid cell by an experienced data analyst. The data chips associated with the detected anomalies were then processed in an automatic processing mode of UX-Analyze. The results of the automatic processing were then reviewed in UX-Analyze's interactive mode to allow operator experience to be included in the target selection. A small number of additional anomalies were identified by the operator and added to the anomaly list. The anomaly list was then sorted into several categories based on the extracted fit parameters. Some of these categories could be immediately excluded from further study as the munitions of interest could not produce such a response. The collection of the anomalies in the remaining categories formed the final detection list for the Indirect Fire Area and served as the target list for the Discrimination Array portion of the demonstration. See Section 5.5.5 for further details on the generation of the final target list.

The UX-Analyze environment for anomaly selection and analysis contains two main graphics tools. One displays an interpolated amplitude image of all the data processed at the site for the current survey and allows the analyst to see which grids of the site have been surveyed and to select grids for target analysis. The area selected for analysis is displayed in another graphic window in which the analyst visually selects targets for characterization. In both of these windows there are options for changing the view area, the mapping color palette and contrast, the amount of information overlaid on the screen, etc. To characterize a target the analyst first



selects the magnetic anomaly by drawing a boundary around the anomaly using the mouse. When the boundary is closed the data inside are sent to a dipole fitting algorithm to determine target location, depth and apparent size.

### 6.3 PARAMETER ESTIMATION

The raw signature data from the TEM array reflect details of the sensor/target geometry as well as inherent EMI response characteristics of the targets themselves. In order to separate out the intrinsic target response properties from sensor/target geometry effects we invert the signature data to estimate principal axis magnetic polarizabilities for the targets. The TEM data are inverted using the standard induced dipole response model wherein the effect of eddy currents set up in the target by the primary field is represented by a set of three orthogonal magnetic dipoles at the target location [14]. The measured signal is a linear function of the induced dipole moment  $\mathbf{m}$ , which can be expressed in terms of a time dependent polarizability tensor  $\mathbf{B}$  as

$$\mathbf{m} = \mathbf{U}\mathbf{B}\mathbf{U}^T \cdot \mathbf{H}_0$$

where  $\mathbf{U}$  is the transformation matrix between the physical coordinate directions and the principal axes of the target and  $\mathbf{H}_0$  is the primary field strength at the target. The eigenvalues  $\beta_i(t)$  of the polarizability tensor are the principal axis polarizabilities.

Given a set of measurements of the target response with varying geometries or "look angles" at the target, the data can be inverted to determine the (X,Y,Z) location of the target, the orientation of its principal axes ( $\phi, \theta, \psi$ ), and the principal axis polarizabilities ( $\beta_1, \beta_2, \beta_3$ ). The basic idea is to search out the set of nine parameters (X,Y,Z, $\phi, \theta, \psi, \beta_1, \beta_2, \beta_3$ ) that minimizes the difference between the measured responses and those calculated using the dipole response model.

For the TEM array data, inversion is accomplished by a two-stage method. In the first stage, the target's (X,Y,Z) dipole location is solved for non-linearly. At each iteration within this inversion, the nine element polarizability tensor ( $\mathbf{B}$ ) is solved linearly. We require that this tensor be symmetric; therefore, only six elements are unique. Initial guesses for X and Y are determined by a signal-weighted mean. The routine normally loops over a number of initial guesses in Z, keeping the result giving the best fit as measured by the chi-squared value. The non-linear inversion is done simultaneously over all time gates, such that the dipole (X,Y,Z) location applies to all decay times. At each time gate, the eigenvalues and angles are extracted from the polarizability tensor.

In the second stage, six parameters are used: the three spatial parameters (X,Y,Z) and three angles representing the yaw, pitch, and roll of the target (Euler angles  $\phi, \theta, \psi$ ). Here the eigenvalues of the polarizability tensor are solved for linearly within the 6-parameter non-linear inversion. In this second stage both the target location and its orientation are required to remain constant over all time gates. The value of the best fit X, Y, and Z from the first stage, and the median value of the first-stage angles are used as an initial guess for this stage. Additional loops over depth and angles are included to better ensure finding the global minimum.

Figure 6-1 shows an example of the principal axis polarizabilities determined from TEM array data. The target, a mortar fragment, is a slightly bent plate about ½ cm thick, 25 cm long and 15 cm wide. The red curve is the polarizability when the primary field is normal to the surface of the plate, while the green and blue curves correspond to cases where the primary field is aligned along each of the edges.

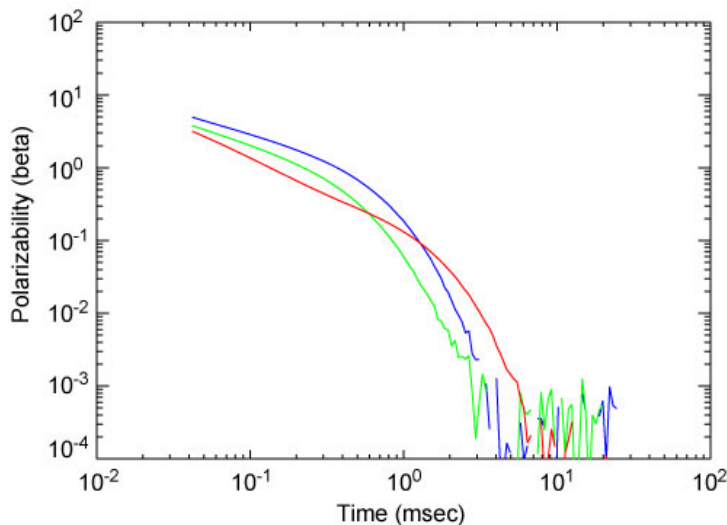


Figure 6-1 – Principal axis polarizabilities for a ½ cm thick by 25cm long by 15cm wide mortar fragment.

Not every target detected during the magnetometer survey had a strong enough TEM response to support extraction of target polarizabilities. All of the data were run through the inversion routines, and the results were manually screened to identify those targets that could not be reliably classified. Several criteria were used in this process: signal strength relative to background, dipole fit error (difference between data and model fit to data), the visual appearance of the polarizability curves. We investigated constraining the depth in the TEM fits using the magnetometer-derived depth. However, a comparison between the derived depths from both systems with the Calibration Grid ground truth showed no significant difference between the two, as shown in Figure 6-2. Further, performing constrained inversions on a subset of our data showed generally negligible change from the non-constrained results. We thus decided not to constrain the TEM depths.

For moderate-to-good SNR, our derived polarizabilities can be directly compared with those of our target library, as shown in Figure 5-5 through Figure 5-7. In these cases, a metric was computed based on how well the amplitude and ratio of the target polarizabilities match those of library objects. The metric runs from 0 (terrible match) to 1 (perfect match). However, for targets with lower SNR, or for cases where a visual inspection suggested a match, but the match quality was below our cutoff, target classification and discrimination were done using library matching procedures similar to those used by Sky Research, Lawrence Berkeley Lab and ourselves in the ESTCP Discrimination Study Pilot Program. In our version, we compare the

quality of an unconstrained dipole inversion of the TEM array data to the quality of a dipole fit constrained by a set of principal axis polarizabilities drawn from a signature library. Fit quality is the squared correlation coefficient between the model fit and the data. If the ratio of the constrained fit quality to the unconstrained fit quality ( $\rho$ ) is one, then the library item is as good a match to the data as possible. If the ratio is small, then the library item is a poor match.

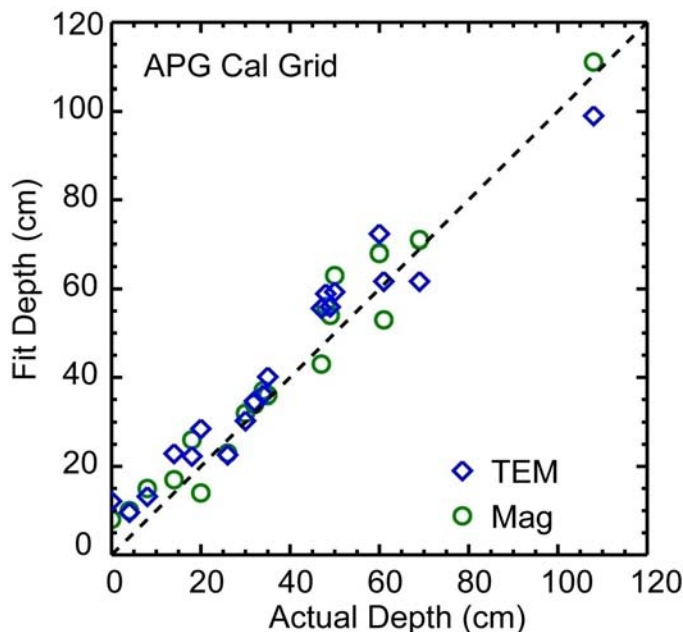


Figure 6-2 – Accuracy of depth estimates from TEM array ( $1\sigma = 6.1$  cm) compared to MTADS magnetometer array ( $1\sigma = 5.4$  cm)

## 6.4 TRAINING

Prior to the demonstration we collected training data in air for all of the 14 standard APG ordnance targets. These data were used to generate the fit library entries. Many of the targets are composites of two or more distinct parts, like a steel body combined with an aluminum tail assembly. Depending on the distance between the sensors and the target, such items can exhibit a range of slightly different EMI signatures corresponding to excitation from different directions. We included measurements with the target oriented nose up, towards the sensor array, nose down, away from the array, flat and obliquely in the fit library.

Our experience at our Blossom Point test site has been that polarizabilities determined from in-air measurements are indistinguishable from those determined from measurements taken over buried targets. We used the data collected from the APG Calibration Area, which contains several instances of each target, to establish that this held true at APG.

We have assembled a fairly extensive polarizability database for clutter items recovered from several different sites. This library was used as training data for establishing UXO/clutter discrimination boundaries on the direct match metric and on the coherence ratio  $\rho$ .

## **6.5 CLASSIFICATION**

As noted in Section 6.3, for anomalies with moderate-to-good SNR and no serious overlap issues, classification was done using the direct match metric, wherein the unconstrained polarizabilities are compared with those of library objects. We had previously assembled a target signature library of the ordnance types present at APG, and supplemented it where necessary with measurements of test objects performed on-site. Using the results of the Calibration Grid, and even considering Blind Grid and IDF anomalies where the visual match to a library object is so good that we have high confidence in the identification, we determined a cutoff value for our metric of 0.56 (reduced to 0.44 for the 25 mm), above which the target is considered ordnance, and below which it is considered clutter. This can be considered a first pass for classification, and was applied to all anomalies.

A number of targets had poorer SNR, but were still amenable to analysis. For these cases, we used the coherence ratio  $\rho$  in conjunction with the direct match metric as our classifier. Library constrained inversions were performed on all these targets, and were also applied to a control group consisting of clean ordnance and clutter targets from the Calibration Grid. For each library inversion, we determine the library object which best fits the current target. We then form the value  $\rho$ , equal to the ratio of the coherence of this fit to that of the unconstrained fit. From analysis of the control group results, a cutoff  $\rho$  of 0.9815 was determined, above which all control group targets are ordnance, and below which they are all clutter. This cutoff was then applied to the poorer SNR targets such that any target which had a value of  $\rho$  equal to or greater than 0.9815 was classified as ordnance, regardless of the value of its direct match metric.

## **6.6 DATA PRODUCT SPECIFICATION**

The demonstration was conducted at the APG Standardized Test Site. We used the standard reporting templates for the Blind Grid and the Open Field shown below in Figure 6-3 and Figure 6-4. The metrics in Section 3.0 were calculated directly from the Scoring Report provided by the Standardized Test Site administrators. The Response Stage value was the maximum signal level above background from the magnetometer anomaly. The calculation of the discrimination stage was more involved. For those targets classified as ordnance, the direct match metric was used as the ranking. Additionally, targets which we could not analyze as described in Section 6.3 were classified as ordnance, but given the lowest confidence rating, and noted as such in our submission. For targets classified as clutter, a division was made between targets that had moderate-to-good SNR and little to no overlap with adjacent targets, and those with either low SNR or more serious overlap issues. For the former class, ranking was based on the direct match metric, while for the latter, ranking was based on a combination of the direct match metric and the peak signal. Classification and Type will be determined from the direct match metric or the

coherence ratio  $\rho$ , as applicable. Easting, Northing, Depth, Azimuth and Dip all come from the dipole inversion results.

BLIND TEST GRID										
	Letter	Number	Response Stage	Discrimination Stage/Ranking	Classification (Use B for Blank)	TYPE	Depth (m)	Azimuth (Degrees)	Dip (Degrees)	Comments
1	A	1								
2	A	2								
3	A	3								
4	A	4								
5	A	5								
6	A	6								
7	A	7								
8	A	8								
...	...	...								

Figure 6-3 – Reporting Template for APG Blind Grid.

INDIRECT FIRE										
	Northing	Easting	Response Stage	Discrimination Stage/Ranking	Classification	TYPE	Depth (m)	Azimuth (Degrees)	Dip (Degrees)	Comments
1										
2										
3										
4										
5										
6										
7										
8										
...										

Figure 6-4 – Reporting Template for APG Indirect Fire Area.

## **7.0 PERFORMANCE ASSESSMENT**

The TEMTADS array was constructed in 2007 and field tested at the APG Standardized UXO Test Site in June 2008 [12]. For the APG demonstration, a magnetometer data set collected the previous month at the newly reconfigured test site was used for anomaly detection in the manner described in the Magnetometer / MkII Demonstration Plan. Approximately 200 cells in the Blind Grid and 700 anomalies in the Indirect Fire Area were interrogated with the TEMTADS, averaging 200 anomalies/day on the Indirect Fire Area. After processing, ranked dig lists were generated and submitted to ATC for scoring.

The performance objectives for this demonstration were summarized in Table 3-1, and are repeated here as Table 7-1 with an additional column indicating whether or not success was achieved. The results for each criterion are then discussed in the following sections. The ATC scoring report for the demonstration, Reference 12, provides the source material for evaluating several of the performance objectives.

Table 7-1 – Performance Results for This Demonstration

Performance Objective	Metric	Data Required	Success Criteria	Success?
<b>Quantitative Objectives</b>				
Reduction of False Alarms	Number of false alarms eliminated at demonstrator operating point.	<ul style="list-style-type: none"> <li>• Prioritized dig list</li> <li>• Scoring report from APG</li> </ul>	Reduction of false alarms by > 50% with 95% correct identification of munitions	Yes
Location Accuracy	Average error and standard deviation in both axes for interrogated items	<ul style="list-style-type: none"> <li>• Estimated location from analysis</li> <li>• Scoring report from APG</li> </ul>	$\Delta N$ and $\Delta E < 10$ cm $\sigma N$ and $\sigma E < 15$ cm	Yes
Production Rate	Number of targets interrogated each day	<ul style="list-style-type: none"> <li>• Log of field work</li> </ul>	75 targets per day	Yes
Analysis Time	Average time required for inversion and classification	<ul style="list-style-type: none"> <li>• Log of analysis work</li> </ul>	15 min per target	Yes
<b>Qualitative Objectives</b>				
Ease of Use		<ul style="list-style-type: none"> <li>• Feedback from operator on ease of use</li> </ul>	Operator comes to work smiling	Yes

## 7.1 OBJECTIVE: REDUCTION OF FALSE ALARMS

This is the primary measure of the effectiveness of this technology. By collecting high-quality, precisely-located data, we expect to be able to discriminate munitions from scrap and frag with high efficiency.

### 7.1.1 Metric

At a seeded test site such as the APG standardized test site, the metric for false alarm elimination is straightforward. We prepared a ranked dig list for the targets we interrogated with a dig/no-dig threshold indicated and ATC personnel use their automated scoring algorithms to assess our results.

### 7.1.2 Data Requirements

The identification of most of the items in the test field is known to the test site operators. Our ranked dig list is the input for this standard and ATC's standard scoring is the output.

### 7.1.3 Success Criteria

The objective will be considered to be met if more than 50% of the non-munitions items can be labeled as no-dig while retaining 95% of the munitions items on the dig list.

### 7.1.4 Results

This Objective was successfully met. The TEMTADS surveyed anomalies detected by the MTADS magnetometer system in the Blind Grid and Indirect Fire Areas. For the Blind Grid Test Area, the discrimination stage results are summarized in Table 7-2 and Table 7-3 (subsets of Table 6a of Reference 12), broken out by munitions type and emplacement depth. For the Indirect Fire Test Area, the discrimination stage results are summarized in Table 7-4 and Table 7-5 (subsets of Table 6c of Reference 12), broken out by munitions type and emplacement depth. The Probability of Detection,  $P_d^{disc}$ , is defined as the number of discrimination-stage detections / number of emplaced munitions in the test site. The Probability of False Positive,  $P_{fp}^{disc}$ , is defined as the (number of discrimination stage false positives)/(number of emplaced clutter items).

Table 7-2 – TEMTADS Blind Grid Test Area  $P_d^{disc}$  Results

$P_d^{disc}$	All Types	105-mm	81/60mm	37/25-mm
Munitions Scores	0.97	0.93	0.97	1.00
0 to 4D	1.00	1.00	1.00	1.00
4D to 8D	1.00	1.00	1.00	1.00
8D to 12D	0.67	0.67	0.00	1.00

Table 7-3 – TEMTADS Blind Grid Test Area  $P_{fp}^{disc}$  Results

$P_{fp}^{disc}$	All Masses	0 to 0.25 kg	>0.25 to 1 kg	>1 to 10 kg
All Depths	0.01	0.02	0.00	0.00
0 to 0.15m	0.01	0.02	0.00	0.00
0.15 to 0.3m	0.00	0.00	0.00	0.00
0.3 to 0.6m	N/A	N/A	N/A	N/A



Table 7-4 – TEMTADS Indirect Fire Test Area  $P_d^{disc}$  Results

$P_d^{disc}$	All Types	105-mm	81/60mm	37/25-mm
Munitions Scores	0.92	0.93	0.93	0.91
By Density				
High	0.88	0.92	0.91	0.80
Medium	0.94	0.97	0.89	0.97
Low	0.94	0.90	0.97	0.94
By Depth				
0 to 4D	0.96	0.94	0.97	0.97
4D to 8D	0.92	0.94	0.92	0.86
8D to 12D	0.72	0.75	0.78	0.67

Table 7-5 – TEMTADS Indirect Fire Test Area  $P_{fp}^{disc}$  Results

$P_{fp}^{disc}$	All Masses	0 to 0.25 kg	>0.25 to 1 kg	>1 to 10 kg
All Depths	0.04	0.03	0.02	0.11
0 to 0.15m	0.04	0.04	0.02	0.13
0.15 to 0.3m	0.04	0.00	0.06	0.06
0.3 to 0.6m	0.08	0.00	0.00	0.20

Efficiency (E) and false positive rejection rate ( $R_{fp}$ ) are used to score discrimination performance ability at two specific operating points on a ROC curve: one at the point where no decrease in  $P_d$  is incurred and the other at the operator-selected threshold. Efficiency is defined as the fraction of detected ordnance correctly classified as ordnance and the false positive rejection rate is defined as the fraction of detected clutter correctly classified as clutter. The results for the Blind Grid and Indirect Fire Test Areas are summarized in Table 7-6 and Table 7-7, from Tables 7a and 7c of Reference 12.

Table 7-6 – TEMTADS Blind Grid Test Area Efficiency and Rejection Rates

	Efficiency (E)	False Positive Rejection Rate
At Operating Point	0.99	0.99
With No Loss of $P_d$	1.00	0.95

Table 7-7 – TEMTADS Indirect Fire Test Area Efficiency and Rejection Rates

	<b>Efficiency (E)</b>	<b>False Positive Rejection Rate</b>
At Operating Point	0.98	0.92
With No Loss of $P_d$	1.00	0.58

## **7.2 OBJECTIVE: LOCATION ACCURACY**

An important measure of how efficiently any required remediation will proceed is the accuracy of predicted location of the targets marked to be dug. Large location errors lead to confusion among the UXO techs assigned to the remediation costing time and often leading to removal of a small, shallow object when a larger, deeper object was the intended target.

### **7.2.1 Metric**

As above, the metric for location accuracy is straightforward at a seeded test site such as the APG standardized test site. We provided an estimated position for all targets we interrogated and ATC personnel used their automated scoring algorithms to assess our results.

### **7.2.2 Data Requirements**

The location of most of the items in the test field is known to the test site operators. Our dig list is the input for this standard and ATC's standard scoring is the output.

### **7.2.3 Success Criteria**

The objective will be considered to be met if the average position error was less than 10 cm in both dimensions (low bias) and the standard deviation of each dimension was less than 15 cm (accurate location).

### **7.2.4 Results**

This Objective was successfully met. The location accuracy of fit parameters generated from the Discrimination Array data are given in Table 7-8 and Table 7-9, taken from Tables 9a and 9c of Reference 12. Horizontal errors are not calculated for the Blind Grid.

Table 7-8 – TEMTADS Blind Grid Test Area Location Error and Standard Deviation

	<b>Mean (m)</b>	<b>Standard Deviation (m)</b>
Northing	N/A	N/A
Easting	N/A	N/A
Depth	0.02	0.04

Table 7-9 – TEMTADS Indirect Fire Test Area Location Error and Standard Deviation

	<b>Mean (m)</b>	<b>Standard Deviation (m)</b>
Northing	0.01	0.05
Easting	0.01	0.05
Depth	0.00	0.06

### 7.3 OBJECTIVE: PRODUCTION RATE

Even if the performance of the technology on the two metrics above is satisfactory, there is an economic metric to consider. There is a known cost of remediating a suspected munitions item. If the cost to interrogate a target is greater than this cost, the technology will be useful only at sites with special conditions or target values. Note, however, that in its ultimate implementation this technology will result in reacquisition, cued interrogation, and target flagging in one visit to the site.

#### 7.3.1 Metric

The number of targets interrogated per day is the metric for this objective. Combined with the daily operating cost of the technology this gives the per-item cost.

#### 7.3.2 Data Requirements

Survey productivity was determined from a review of the ATC demonstration field logs.

#### 7.3.3 Success Criteria

For this first demonstration, the objective will be considered to be met if at least 75 targets were interrogated each survey day.

#### 7.3.4 Results

This Objective was successfully met. Data collection times are taken from Table 5 of Reference 12. For the purposes of this discussion, a typical work day is assumed to be 7 hours of active

data collection and 1 hour of daily setup and tear down. 214 anomalies were investigated on the Blind Grid over the course of 10 hours and 3 minutes, or 1.43 work days, or on average 149 anomalies / work day. 694 anomalies were investigated in the Indirect Fire Area over the course of 32 hours and 30 minutes, or on average 150 anomalies / work day. In fact, through the generosity of the ATC staff, we were able to work for ten or more hours on several days and achieved production rates of > 220 anomalies / day for three days at the end of the first week of the demonstration.

## **7.4 OBJECTIVE: ANALYSIS TIME**

The ultimate implementation of this technology will involve on-the-fly analysis and classification. The time for this will be limited to the driving time to the next anomaly on the list. We tracked the near-real-time analysis time in this demonstration.

### **7.4.1 Metric**

The time required for inversion and classification per anomaly is the metric for this objective

### **7.4.2 Data Requirements**

Analysis time will be determined from a review of the data analysis logs.

### **7.4.3 Success Criteria**

For this first demonstration, the objective will be considered to be met if the average inversion and classification time was less than 15 min.

### **7.4.4 Results**

This Objective was successfully met. The average inversion time per target was approximately 2.5 minutes on our field laptop computer. Including this, the average analysis time amounted to 12.5 minutes per anomaly. Since this was the first extensive test of the system in field mode, we took the opportunity to consider various discrimination and classification methods, some of which proved unfruitful. As a result of lessons learned from this undertaking, we expect the average analysis time for future field runs to be less than that obtained here.

## **7.5 OBJECTIVE: EASE OF USE**

This qualitative objective is intended as a measure of the long-term usability of the technology. If the operator does not report that the technology is easy to use, shortcuts that can compromise the efficiency of the technology will begin to creep into daily operations.

### **7.5.1 Data Requirements**

This objective was evaluated based on operator feedback.

## 7.5.2 Results

This Objective was successfully met. Based on vehicle operator feedback, there were no significant limitations to the efficient use of the system in the field. Several suggestions were made for additional improvements to the navigation and data collection software. They have been subsequently incorporated. Based on the discussion in 5.5.14, anomalies for future demonstrations will be ordered along 1m swaths for maximum data collection efficiency.

## 8.0 SCHEDULE OF ACTIVITIES

Figure 8-1 gives the overall schedule for the demonstration including deliverables.

	Activity Name	2008					
		Mar	Apr	May	Jun	Jul	Aug
1	APG Demonstration						
2	Draft Demonstration Plan						
3	Final Demonstration Plan						
4	Magnetometer Data Collection						
5	Discrimination Data Collection						
6	Data Analysis						
7	Ranked Dig Lists to ATC						
		March	April	May	June	July	August

Figure 8-1 – Schedule for all demonstration activities including deliverables.

## 9.0 MANAGEMENT AND STAFFING

The responsibilities for this demonstration are outlined in Figure 9-1. Tom Bell and Dan Steinhurst are the co-PIs of this project and jointly filled the roles of Site / Project Supervisor. Glenn Harbaugh was the Site Safety Officer and Data Acquisition Operator. His duties included data collection and safety oversight for the entire team. Dan Steinhurst assisted with data collection and served as the Data Analyst for the magnetometer survey. Tom Bell served as the Quality Assurance Officer for this demonstration and oversaw the Data Analysts. Data analysis support for the Discrimination Array data collection effort was provided by Jim Kingdon.

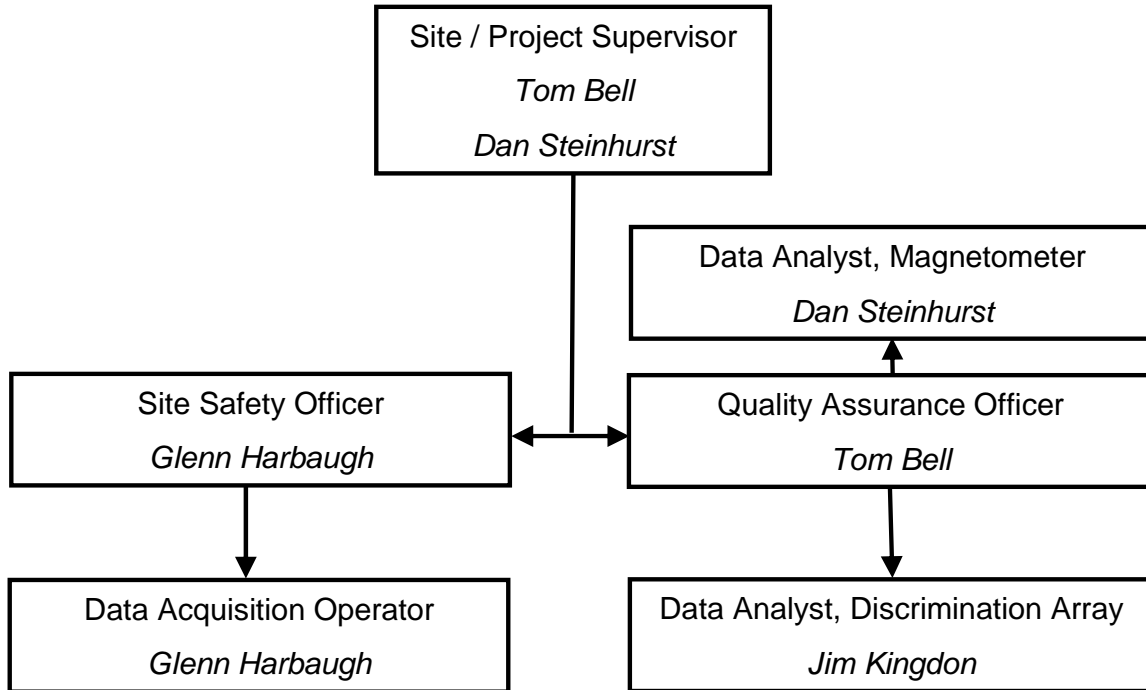


Figure 9-1 – Demonstration management and staffing diagram.

## 10.0 REFERENCES

1. "Report of the Defense Science Board Task Force on Unexploded Ordnance," December 2003, Office of the Under Secretary of Defense for Acquisition, Technology, and Logistics, Washington, D.C. 20301-3140, <http://www.acq.osd.mil/dsb/uxo.pdf>.
2. <http://aec.army.mil/usaec/technology/jpgphaseiv.pdf>.
3. "Standardized UXO Technology Demonstration Site Blind Grid Scoring Record No. 39," <http://aec.army.mil/usaec/technology/uxo-record39.pdf>.
4. Foley, J. E., M. Miele, R. Mehl, J. Dolynchuk, J. Hodgson and J. Swanson, "Procedures for Applying UXO Discrimination Technology at the Former Lowry Bombing and Gunnery Range," UXO/Countermines Forum, Saint Louis, March 9-12, 2004.
5. Aberdeen Proving Ground Soil Survey Report, October 1998.
6. Nelson, H. H. and Steinhurst, D. A., "MTADS Geophysical Survey of the ATC Standardized UXO Technology Demonstration Site Proposed Active Response Area," Naval Research Laboratory Letter Report Number 6110-089, August 6, 2003.
7. Harbaugh, G.R., Steinhurst, D.A., and Khadr, N., "MTADS Demonstration at Camp Sibert Magnetometer / EM61 MkII / GEM-3 Arrays," Demonstration Data Report, September 26, 2007.
8. Steinhurst, D., Khadr, N., Barrow, B., and Nelson, H. "Moving Platform Orientation for an Unexploded Ordnance Discrimination System," GPS World, 2005, 16/5, 28 – 34.
9. Nelson, H. H., "Array Specification Report," ESTCP MM-0601, June, 2007.
10. Nelson, H. H., ESTCP In-Progress Review, Project MM-0601, March 1, 2007.
11. Nelson, H. H. and Robertson, R., "Design and Construction of the NRL Baseline Ordnance Classification Test Site at Blossom Point," Naval Research Laboratory Memorandum Report NRL/MR/6110—00-8437, March 20, 2000.
12. "STANDARDIZED UXO TECHNOLOGY DEMONSTRATION SITE SCORING RECORD NO. 920 (NRL)," J.S. McClung, ATC-9843, Aberdeen Test Center, MD, November, 2008.
13. Bell, T., Barrow, B., Miller, J., and Keiswetter, D., "Time and Frequency Domain Electromagnetic Induction Signatures of Unexploded Ordnance," Subsurface Sensing Technologies and Applications Vol. 2, No. 3, July 2001.

14. Bell, T. H., Barrow, B. J., and Miller, J. T., "Subsurface Discrimination Using Electromagnetic Induction Sensors," IEEE Transactions on Geoscience and Remote Sensing, Vol. 39, No. 6, June 2001.



## Appendix A: Points of Contact

<b>POINT OF CONTACT</b>	<b>ORGANIZATION</b>	<b>Phone Fax e-mail</b>	<b>Role in Project</b>
Dr. Jeff Marqusee	ESTCP Program Office 901 North Stuart Street, Suite 303 Arlington, VA 22203	703-696-2120 (V) 703-696-2114 (F) jeffrey.marqusee@osd.mil	Director, ESTCP
Dr. Anne Andrews	ESTCP Program Office 901 North Stuart Street, Suite 303 Arlington, VA 22203	703-696-3826 (V) 703-696-2114 (F) anne.andrews@osd.mil	Deputy Director, ESTCP
Dr. Herb Nelson	ESTCP Program Office 901 North Stuart Street, Suite 303 Arlington, VA 22203	703-696-3726 (V) 703-696-2114 (F) 202-215-4844 (C) herbert.nelson@osd.mil	Program Manger, MM
Ms. Katherine Kaye	HydroGeoLogic, Inc. 11107 Sunset Hills Road, Suite 400 Reston, VA 20190	410-884-4447 (V) kkaye@hgl.com	Program Manager Assistant, MM
Dr. Dan Steinhurst	Naval Research Lab Chemistry Division Code 6110 Washington, DC 20375	202-767-3556 (V) 202-404-8119 (F) 703-850-5217 (C) dan.steinhurst@nrl.navy.mil	Co-PI and Data Analyst
Mr. Glenn Harbaugh	Army Research Lab Building 512 Blossom Point Rd. Welcome, MD 20693	804-761-5904 (V) glenn.harbaugh@nrl.navy.mil	Site Safety Officer
Dr. Tom Bell	SAIC 200 12th Street South Arlington, VA 22202	703-414-3904 (V) 703-413-0505 (F) 301-712-7021 (C) thomas.h.bell@saic.com	Co-PI and Quality Control Officer
Dr. Jim Kingdon	SAIC 200 12th Street South Arlington, VA 22202	703-414-3872 (V) 703-413-0505 (F) james.b.kingdon@saic.com	Disc. Array Data Analyst
Mr. Rick Fling	Aberdeen Test Center	410-278-2999 (V) 301-992-9080 (C) rick.fling@us.army.mil	Test Site Manager



## Appendix B: Data Formats

The MTADS Discrimination Array is a new sensor system and the file formats have not been discussed elsewhere. The contents of the two data files collected for each anomaly and a brief explanation of each entry are provided below.

### Position (.GPS) Files

```
Antenna,X_Offset,Y_Offset,Z_Offset,Easting/Yaw,Northing/Pitch,HAE/Range
Main,0.000,1.365,0.730,316256.990,4254211.094,-25.934
AVR1,-0.778,-1.418,0.740,3.40349,0.00761,2.882
AVR2,0.778,-1.418,0.745,1.55718,0.00425,1.554
```

These data files are ASCII format, comma-delimited files. A header line is provided.

Line 1 – Header information

Line 2 – Main GPS antenna data

Main	- Antenna Identifier
0.000	- Cross-track distance from array center
1.365	- Down-track distance from array center
0.730	- Vertical distance from array center
316256.990	- Easting (UTM, m) position of Main antenna
4254211.094	- Northing (UTM, m) position of Main antenna
-25.934	- Height-above-ellipsoid (m) position of Main antenna

Line 3 & 4 – AVR GPS antenna data (AVR1 as example)

AVR1	- Antenna Identifier
-0.778	- Cross-track distance from array center
-1.418	- Down-track distance from array center
0.740	- Vertical distance from array center
3.40349	- Yaw of AVR vector (radians, True North referenced)
0.00761	- Pitch of AVR vector (radians)
2.882	- Range of AVR vector (m)

### Sensor (.TEM) Files

These data files are a binary format generated by a custom .NET serialization routine. They are converted to an ASCII, comma-delimited format in batches as required. Each file contains 25 data points, corresponding to each Tx cycle. Each data point contains the Tx transient and the corresponding 25 Rx transients as a function of time. A pair of header lines is also provided for, one overall file header and one header per data point with the data acquisition parameters. A partial example is provided below.

## Line 1 - File Header

CPUsms,PtNo,LineNo,Delt,BlockT,nRepeats,DtyCyc,nStk,AcqMode,GateWid,GateHOff,T  
xSeq,GateT,TxI\_Z,Rx0Z\_TxZ,Rx1Z\_TxZ,Rx2Z\_TxZ,Rx3Z\_TxZ,Rx4Z\_TxZ,Rx5Z\_TxZ,Rx6Z\_T  
xZ,Rx7Z\_TxZ,Rx8Z\_TxZ,Rx9Z\_TxZ,Rx10Z\_TxZ,Rx11Z\_TxZ,Rx12Z\_TxZ,Rx13Z\_TxZ,Rx14Z\_T  
xZ,Rx15Z\_TxZ,Rx16Z\_TxZ,Rx17Z\_TxZ,Rx18Z\_TxZ,Rx19Z\_TxZ,Rx20Z\_TxZ,Rx21Z\_TxZ,Rx22  
Z\_TxZ,Rx23Z\_TxZ,Rx24Z\_TxZ,

## Line 2 - Data Point Header

0,1,0,2E-06,0.9,9,0.5,3,2,0.05,5E-05,22,

0	- Start time in ms on CPU clock (always 0)
1	- Data Point Number (always 1)
0	- Line Number (always 0)
2E-06	- Time step for transients (seconds)
0.9	- Base period length (seconds)
9	- Number of Tx cycles in a base period
0.5	- Duty cycle
3	- Number of base periods averaged (or stacked)
2	- Data Acquisition Mode (binned)
0.05	- Gate width as fraction of its own time
5E-05	- Hold-off time (seconds) for first data point
22	- Tx ID number (sensor number + 10)

## Line 3 - First Data Line in First Data Point

,,,,,,,,,,2.5E-05,2.01102465120852,-4.71949940100108E-05,-  
1.79793904939509E-05,1.39366551389817E-05,-2.55470612811271E-05,-  
4.84779418501355E-05,4.05641650778409E-05,6.73185201421361E-06,-  
0.000116516308079121,-2.49295973312366E-06,4.21216420108736E-  
05,3.70976690069955E-05,-0.000127606649206979,-0.000510366345393333,-  
0.000100251591870083,5.19149917311475E-05,3.71239440686929E-05,-  
6.05368361143584E-06,-0.000125671808025774,2.44747669528873E-  
05,5.7401043406257E-05,-5.14479298585597E-05,-9.42595187481444E-  
06,3.27817636140336E-05,-1.1886747308274E-05,-5.57022247620241E-05,